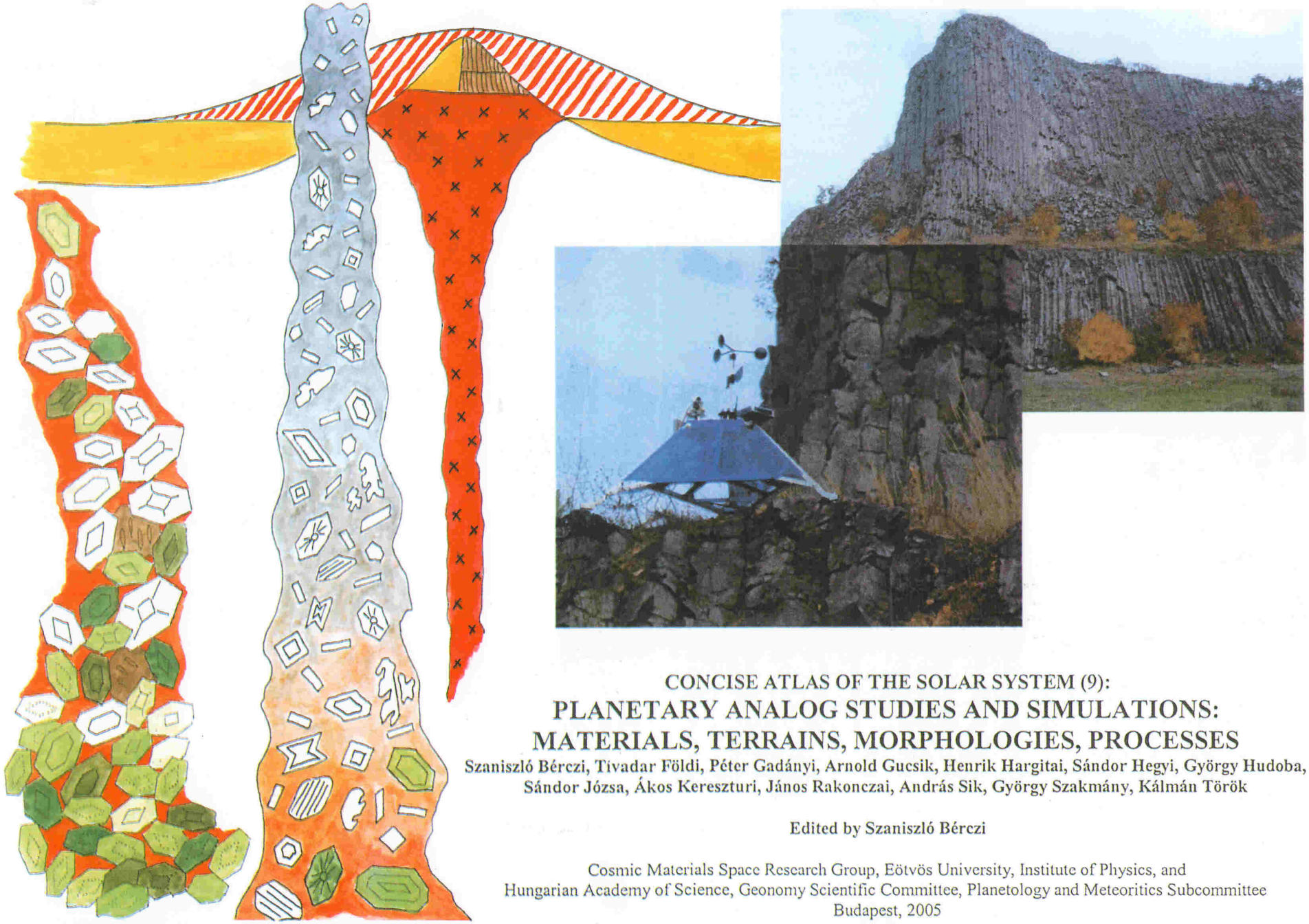

CONCISE ATLAS OF THE SOLAR SYSTEM (9):

PLANETARY ANALOG STUDIES AND SIMULATIONS: MATERIALS, TERRAINS, MORPHOLOGIES, PROCESSES

Szaniszló Bérczi, Tivadar Földi, Péter Gadányi, Arnold Gucsik, Henrik Hargitai, Sándor Hegyi, György Hudoba, Sándor Józsa, Ákos Kereszturi, János Rakonczai, András Sik, György Szakmány, Kálmán Török

Edited by Szaniszló Bérczi

Cosmic Materials Space Research Group, Eötvös University, Institute of Physics, and
Hungarian Academy of Science, Geonomy Scientific Committee, Planetology and Meteoritics Subcommittee
Budapest, 2005

CONCISE ATLAS ON THE SOLAR SYSTEM (9)
PLANETARY ANALOG STUDIES AND SIMULATIONS
MATERIALS, TERRAINS, MORPHOLOGIES, PROCESSES

One of the main planetary educational projects at the Cosmic Materials Space Research Group, working under the auspices of the Faculty of Science, Institute of Physics, Eötvös Loránd University, includes studies of planetary materials, studies of terrains on Earth which are analog with other planetary surface terrains and planetary robotic simulations in reconstructed planetary testfield conditions by the educational space probe models Hunveyor and Husar. These analog studies and simulations help students in discovering the whole system of works, measurements, various activities carried out in real, on site robotic and manned planetary geology.

Analog studies play a key role in comparative planetary geology. Many geologic knowledge origins from terrestrial geology, however, they can be transformed to other planetary conditions if we compare and fit them to the conditions on the other planet. For example principles of stratigraphy were used first on the Moon (Shoemaker, Wilhelms, 1962), but the problem of correlation of distant strata needed introduction a new method of crater statistics instead of fossil records used in Earth. At the same time impact history of planetary bodies were recognized on the basis of other planetary surfaces (Moon, Mars, Mercury, Galilean satellites of Jupiter etc.) and it was fitted to terrestrial impact craters discovered on Earth mainly during the morning decades of planetary science. This mutual development by transfering ideas from terrestrial works to planetary ones can be intensified by analog methods.

Various analog planetary geology studies were organized first for astronauts preparing to the lunar landing in the Apollo Era. American desert and mountainous regions were visited by them in the Grand Canyon and Arizona (Meteor crater) and other sites. Recently the Mars is the main object for manned and robotic research. Mars analog terrains can be found in several places on the Earth. Haughton crater in Devon Island, Canada and Antarctic terrains are cold desert places, where impact processes (Haughton crater) and extremal cold conditions (both places) are present. For analog sites with martian volcanism together with ice, glaciers, ice-lava interactions the islands of Iceland and Svalbard seem excellent places.

For university education the analog studies may extend to various materials, terrains, processes and simulations which are related somehow to planetary ones. We began this work in the Concise Atlas on the Solar System (6): Atlas of Microenvironments on Planetary Surfaces. There mainly the lander works on the surface of the Moon and Mars were overwieved. In this concise atlas (9) new topics are included to planetary analog studies and simulations as follows:

I. Planetary space probe activity simulations

1.1. A Hunveyor type planetary voyage and planetary surface works simulator.

1.2. Hunveyor orientations and astronomical observations on Martian surface.

II. Terrain, morphology, material and process analogies from orbit and planetary surface

2.1. Proposed Europa analog ice-splitting measurements and experiments with ice-Hunveyor on the frozen Balaton-Lake, Hungary.

2.2. Meandering riverbed analogs on Mars and Earth.

2.3. Comparative study of periglacial mass movements on Mars and in Anatolia on Earth

2.4. The interaction of ice and volcanism on the Mars and in Iceland on Earth.

III. Planetary material analog studies

3.1. Martian shergottites and their counterparts from the Szentbékkálla series of mantle lherzolite inclusions and the host basalts in North-Balaton Mountains, Hungary.

3.2. Terrestrial impact melt rock and breccia from the Mien Crater, Ramsö Island central peak, Sweden.

3.3. Impact materials of the Ries Crater, Germany.

3.4. Analog studies on rock assemblages delivered to a plain by floods, on Earth (Dunavarsány) and on Mars (Chryse-plains).

IV. Lunar, Martian, chondritic and achondritic meteorite samples compared to their textural and formation process industrial material analogs

4.1. Textures of basalts and basaltic clasts of the NASA lunar educational set: comparisons to terrestrial basalts.

4.2. Cooling rate sequence of chondrule textures

4.3. Martian nakhlite textural layers in the cumulate pile of a thick flow: terrestrial analog: Theo's flow, Canada.

4.4. Comparison of breccias from the Moon, the Earth, and the asteroids.

4.5. Analog studies on textures: comparison of lunar basalts and breccias with industrial materials of steels and ceramics.

V. Planetary analog terrains and rocks visited on field works in Hungary.

5.1. Igneous rocks and terrain morphology

5.2. Eroded, fluvial, transported rocks and morphology

On the basis of our experiences with the earlier members of this Concise Atlas series we encourage colleagues to develop both their own robotical facilities, test table arrangements and choose favourite measurements which can be realized in some future space probe mission.

The next volumes of this series will cover developments on the Hunveyor-Husar model system, Planetary Science and Physics, Technologies and Inventions in Space Science.

Volumes of the series Concise Atlas on the Solar System:

(1): *Planetary and Material Maps on: Lunar Rocks, Meteorites* (2000);
(2): *Investigating Planetary Surfaces with the Experimental Space Probe Hunveyor Constructed on the Basis of Surveyor* (2001); (E)
(3): *Atlas of Planetary Bodies* (2001); (E)
(4): *Atlas of Planetary Atmospheres* (2002);
(5): *Space Research and Geometry* (2002);
(6): *Atlas of Micro Environments of Planetary Surfaces* (2003); (E)
(7): *Atlas of Rovers and Activities on Planetary Surfaces* (2004);
(8): *Space Research and Chemistry* (2005);
(9): *Planetary Analog Studies and Simulations: Materials, Terrains, Morphologies, Processes*. (2005); (E)
(E) marks the English language editions of the series issues.

Szaniszló Bérczi, Tivadar Földi, Péter Gadányi, Arnold Gucsik, Henrik Hargitai, Sándor Hegyi, György Hudoba, Sándor Józsa, Ákos Kereszturi, János Rakonczai, András Sik, György Szakmány, Kálmán Török

CONCISE ATLAS ON THE SOLAR SYSTEM (9):
PLANETARY ANALOG STUDIES AND SIMULATIONS
MATERIALS, TERRAINS, MORPHOLOGIES, PROCESSES

Szaniszló Bérczi, editor

ISBN 963 00 6314 XÖ
963 86873 2 0

Kiadja az ELTE TTK / MTA Geonómia Bizottság, Kozmikus Anyagokat Vizsgáló Űrkutató Csoport és az UNICONSTANT

E munka megjelentetését a Magyar Űrkutatási Iroda az ELTE TTK / MTA Geonómia Bizottság Kozmikus Anyagokat Vizsgáló Űrkutató Csoport TP-154/2005 számú témapályázata keretében támogatta. E támogatásért a MŰI-nek köszönetet mondunk.

Acknowledgments: The loan of the Lunar Educational Thin Section Set from NASA JSC, Houston, the Antarctic Meteorite Educational Thin Section Set from NIPR, Tokyo, and the fund of MŰI-TP-154/2005 of Hungarian Space Office are highly acknowledged.

Published by the Cosmic Materials Space Research Group of Eötvös University / Geonomy Scientific Committee, Planetology and Meteoritics Subcommittee of the Hungarian Academy of Science, Budapest, 2005

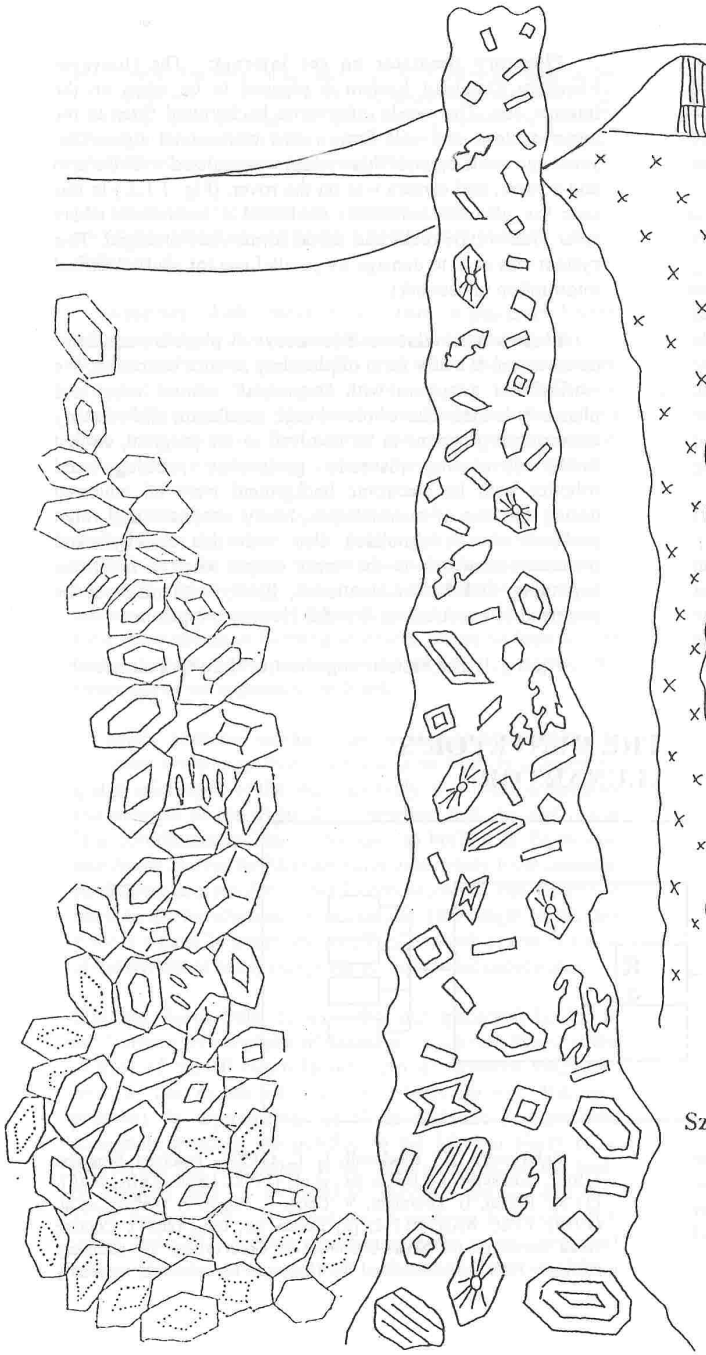

The paragenetic sequence for a lunar basalt: armalcolite, ilmenite, olivine, clinopyroxene and plagioclase feldspar.

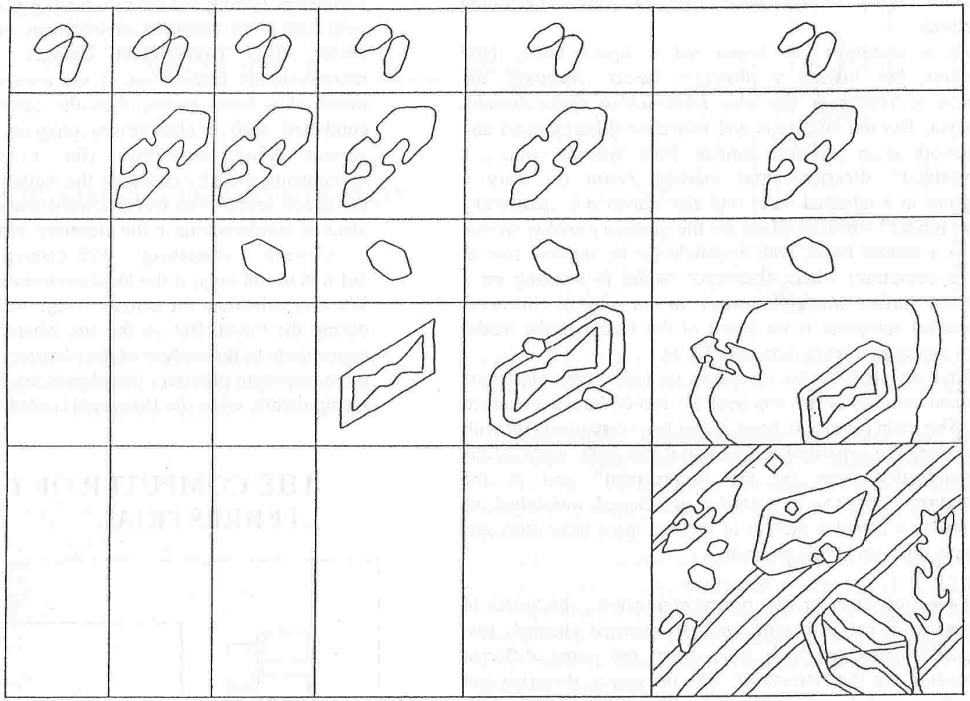

CONCISE ATLAS OF THE SOLAR SYSTEM (9):

PLANETARY ANALOG STUDIES AND SIMULATIONS: MATERIALS, TERRAINS, MORPHOLOGIES, PROCESSES

Szaniszló Bérczi, Tivadar Földi, Péter Gadányi, Arnold Gucsik, Henrik Hargitai, Sándor Hegyi, György Hudoba, Sándor Józsa, Ákos Kereszturi, János Rakonczai, András Sik, György Szakmány, Kálmán Török

Edited by Szaniszló Bérczi

Cosmic Materials Space Research Group, Eötvös University, Institute of Physics, and
Hungarian Academy of Science, Geonomy Scientific Committee, Planetology and Meteoritics Subcommittee

Budapest, 2005

1.1. A HUNVEYOR TYPE PLANETARY VOYAGE AND PLANETARY SURFACE WORKS SIMULATOR.

Introduction: Space Camp, Huntsville, Alabama, every year organizes International Space Camp, a week program for students and teachers [1]. There many Hungarian students could visit the various programs in which many space simulators work. That is why that attention of space science education turns toward such type of new educational directions.

As a prototype we began not a Space Camp type simulator, but instead a planetary lander. Although the example to Hunveyor was also from NASA space arsenal: Surveyor. But the electronic and educational background and framework is in principle similar. Both systems contain a **"terrestrial" direction and control room** (or only a computer in a minimal case) and also contains a **„planetary probe model" working place** for the planetary analog works. This is a second room, with a tesfield (or in minimal case at least a computer) where Hunveyor model is working on a planetary surface (metaphorically). In our case of Hunveyor the second computer is on board of the lander probe model which serves as a space simulator [2, 3].

First we describe the system in its basic main electronic form and some activities and possible combinations are added later. The main electronic basis is that two computers talk with each other. The benefit of this system is that both "ends" of the communication line: (at the **"terrestrial"** and at the **"planetary"** one) can be extended, developed, multiplied, so that finally a complex system of various space simulators can be made grow up in this program.

Two computers in two rooms connected: The hearth of the system is the following communicational channel: two computers connected with each other, but using different peripheries. On the "terrestrial" side the active, directing and controlling peripheries are dominant (joystick, claviatures, monitors) while on the "planetary" side the sensorial, manipulator peripheries are dominant. In an on line connections the RS 232 ports of the PC-s were used for the connection [4]. (Fig. 1.1.1.)

Planetary simulator in work: Planetary simulator is interesting even if it is in its constructional stage. A whole travel must be planned, from launch till landing, and from beginning of instrumental works till the manipulating works carried out. Like as in the Space Camp programs various accidents, failures, mistakes can be programmed. For example in a Martian case a dust storm, or snow coverage may cause transitional out of work at some instruments. If we work with Hunveyor in a sapce simulator mode we can use the peripheries in new roles. Earlier we planned Hunveyor for scientific instruments construction. But simulating a whole space travel attached new programs to our system. We show some of them.

Peripheries: *During the voyage: camera as travel periphery*: During the travel toward a planetary body the sky with stars is the observed environment with the camera of the lander. This environment changes when mid course maneuvers are carried out. If we want to simulate a whole travel of a lunar probe, then the camera system must be combined with a planetarium program. We may compute various other maneuvers (for example trying some instruments, etc.) by changing the stellar environment around the space probe- The travel toward the planet is an exciting place of combinations in the planetary simulator.

Camera + something: Web camera is everyday artifact but it is useful only, if the local environment is interesting [5]. We may substitute the camera image with planetary program during the travel. But on the site where we landed we must concentrate to the surface of the planetary body. Therefore the most important planetary peripheries are the cameras and little manipulators, when the Hunveyor landed.

Planetary simulator on the internet: The Hunveyor Planetary Simulator System is planned to be taken on the internet, too. This needs informatics background fitted to the larger system, and will form a new educational style. Two years ago some parts of this system was realized with the arm and a rover, and camera was on the rover. (Fig. 1.1.2.) In this case the planetary simulator contained a test-terrain where solar system type rocks and desert forms were arranged. This system was easy to damage by parallel use (or short electrical interruption in network).

Planetary simulators: Summary: A planetary simulator construction is a new form of planetary science education. We worked out a system with "terrestrial" control room and planetary lander. The whole voyage simulation allows many enthusiastic programs to be involved in the program, so that finally astronomy, planetary geography, petrology and robotics with its electronic background were all educated during the use of a simulation. Many astronaut and robot problem can be simulated also with this activity. And planetary simulator is the most simple one. It is at the beginning, and further simulators, finally with man can be practiced by constructing first this Hunveyor type one.

Fig. 1.1.1. The basic arrangement of Hunveyor simulator.

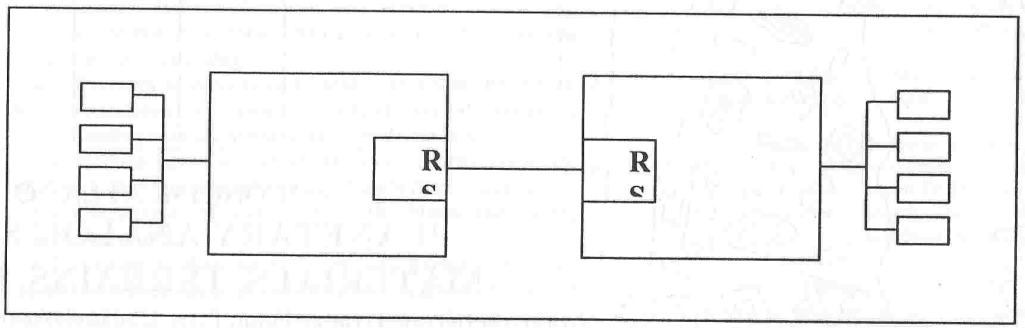

The manipulators and the camera of Surveyor style can be moved with small number of simple DC motors. Even if the power system has not been built by solar panel, the system can work through network, and through controllers. We planned our system for active units with 2 motors each.

References: [1] Blackwell T. L. (1993): Teachers Program. MSFC, Huntsville; [2] Bérczi Sz., et al.. (1998): LPSC XXIX, #1267; [3] Sz. Bérczi, B. Drommer, V. Cech, S. Hegyi, J. Herbert, et al. (1999): LPSC XXX. #1332; [4] Bérczi Sz., (ed.) (2001): Concise Atlas Series of the Solar System (2): Observations on planetary surfaces: How we constructed the Hunveyor experimental university

space probe Hunveyor on the basis of NASA Surveyor lunar lander. (In Hungarian) UNICONSTANT. Budapest-Pécs-Szombathely; [5] Bérczi Sz., Cech V., Hegyi S., Drommer B., Borbola T., Diósy T., Köllő Z., Tóth Sz. (1998): The use of Hunveyor in Antarctic research. *23rd NIPR Symp.Antarctic Meteorites*, Tokyo,. p. 8.

1.2. HUNVEYOR ORIENTATIONS AND ASTRONOMICAL OBSERVATIONS ON MARTIAN SURFACE.

Abstract: With Hunveyor simulator, a planetary lander, with capabilities for observations and orientations on the Martian surface, we studied also orientation and space station activities at the Lagrangian points of the Earth+Sun or Earth+Moon system. The basic coordinate transformations were formulated in this course and the space-orientation requirements for planetary surface robotics were also studied.

Introduction: Developing our Hunveyor system [1,2] we studied: how to orient space probe instruments on Martian surface. How the known terrestrial coordinate systems change and how to develop the necessary transformations for astronaut simulator work. What is a useful spatial orientation for a space station in Lagrangian points, where no local visible bodies except light points on the sky can preserve the environment we acustomed on Earth.

Mars surface works: The most important thing to introduce students to living conditions on Mars is to learn the spatial orientation of the planetary body: that is the orientation and motions of the night sky. Therefore first the real North Pole coordinates of Mars were used to build a II. Equatorial coordinate system for Martian astronauts. Many local calendar parameters are similar or well comparable to the terrestrial ones, so the transformations are simple, (the length of the day = sol is almost 24 hours, the length of a month is almost twice of the terrestrial ones) except the II. Equatorial coordinates.

Martian North Pole: Imagine that our spacecraft landed in the Northern Hemisphere of Mars, in the Chryse Plain, at the vicinity of the 40 North latitude and 45 Western longitude, near to the mouth of Kasei riverbeds (almost Viking-1 position). In reproducing the Horizontal and I. Equatorial coordinate systems, the position of the Martian North polar axis on the sky is neeeded. It has been measured on the basis of Viking-1 and -2, and also Pathfinder missions, and it is 317,7 degrees RA (21 hours and 8 mins in traditional RA units) and +52,9 degrees declination given in our terrestrial system [3]. This position is near to the North America Nebula and Deneb in the Cygnus constellation. Therefore the role of Ursa Minor in spatial orientation on Earth (North. Hempisph.) can be replaced by Cygnus on the surface of Mars (North. Hemisph.)

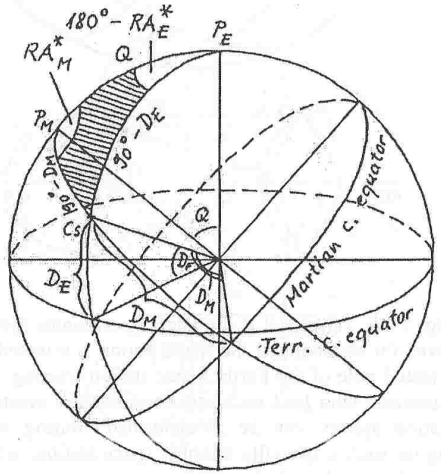

Fig. 1.2.1. Transformations of the II. Equatorial system of Earth to that of Mars.

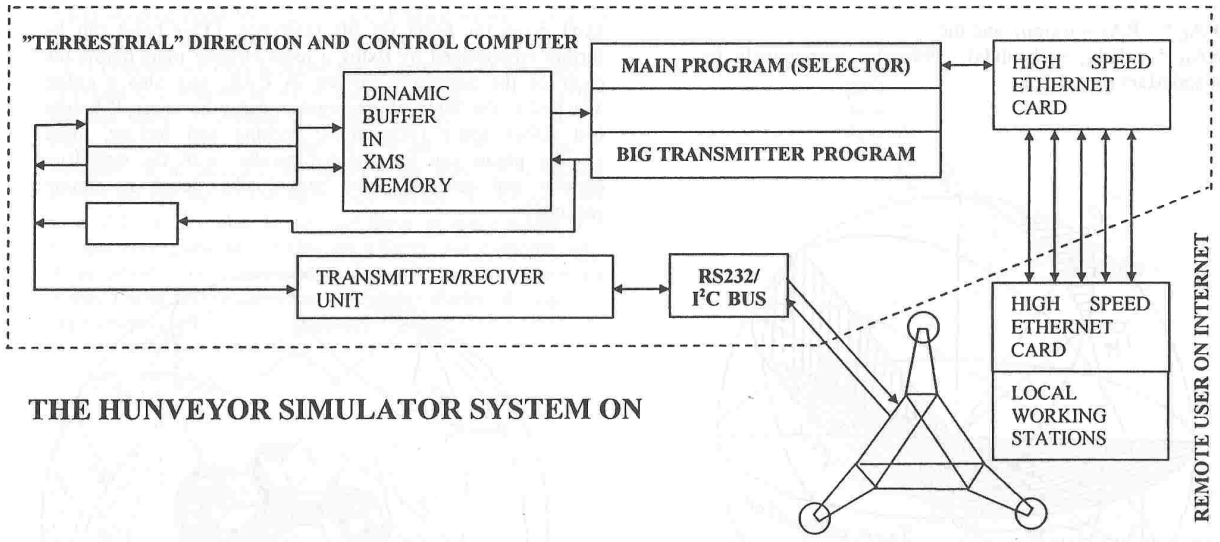

THE HUNVEYOR SIMULATOR SYSTEM ON

Fig. 1.1.2. If the planetary simulator is connected to the internet remote users can keep in contact with the program.

Coordinate transformations to Mars: In spherical coordinate transformations the two N. polar points (of Earth and of Mars) and any of the star positions give the basis of the spherical triangle, where to give the spherical sinus and cosinus theorems.

The arc distance of the two poles is: Q, declination in Terrestrial system D_E, in Martian system D_M (Fig. 1.2.1.) The corresponding complement angles (to 90 degrees) form the two arc-sides of the celestial spherical triangle, together with Q as the third side. The II. Equatorial longitudes of this star are RA_E * and RA_M *

According to sinus theorem:

$$\frac{\sin (90° - D_M)}{\sin (90° - D_E)} = \frac{\sin (180° - RA_E^*)}{\sin RA_M^*}$$

and cosinus theorem:

$$\cos (90° - D_E) =$$
$$\cos (90° - D_M).\ \cos Q + \sin (90° - D_M)\ .\ \sin Q\ .\ \cos RA_M^*$$

Because RA_E * and RA_M * are measured from the spherical circle, which connects the two poles, the real RA_E and RA_M can be transformed by the

$RA_E^* = RA_E + \mu$ (mu) and the
$RA_M^* = RA_M +$ (lambda) formulas, respectively for Earth and Mars (Fig. 1.2.2.)

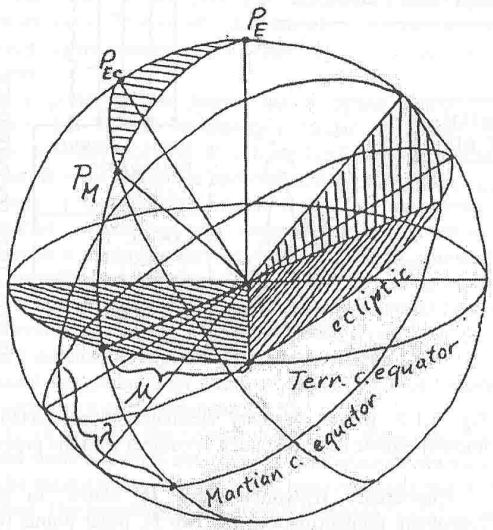

Fig. 1.2.2. Orbital plane relations for Earth and Mars with reference to ecliptic. The coordinates of the Cs star should be transformed to the PE – PM circle by mu before, and by lambda after the spherical triangle transformations to move them to the vernal equinox on the Terrestrial cel. equator and the corresponding Martian ascension node for the Martian cel. equator.

Space station orientation at the Lagrange points: We studied another space orientation simulation, when a space station is placed into one of the Lagrangian points of the Sun-Earth system or the Earth-Moon system. The question was: how can we preserve most knowledge about the terrestrial environment in such a far spatial site from Earth. How to promote astronaut orientation over the local geometry of the space station building itself [4,5].

We simulated the spatial orientation of the space station (slow rotation can preserve many orientation reflex of the astronaut) so that the astronomical equatorial coordinate systems preserved many local characteristics of the Earth body. The projected equator (with the corresponding rotational axis) gives the basis for the reference. (This basis can be further emphasized by fixing a local circular plate below the chair of the astronaut moving in EVA, and also a collar attached to the body of astronaut to sense horizon). If he/she lost stabel space [orientation] sensing and feeling, these circular plates can be adjusted parallel with the terrestrial equator and astronaut gets back his/her local orientation sensing.)

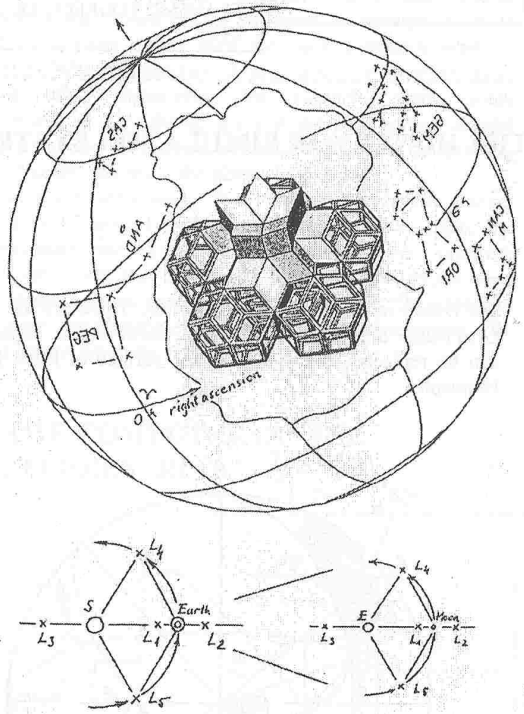

Fig. 1.2.3. Terrestrial II. Equatorial coordinate system can "survive" for astronauts if the space station is oriented toward the celestial pole of the Earth. Space station training is useful for astronauts who land on Mars, because their mental space orientation system can be "transformed" during a month staying on such a specially oriented space station, which can be moved into the Martian polar axis orientation position during the second month staying. All these effects can be prepared in the type of Hunveyor simulator we were working on.

Therefore our experience is that if the orientation for a space station is such type that it preserved the polar axis position of the Earth, (and together with it the terrestrial celestial equator) then the astronauts can use their terrestrial view and always can renormalize their space orientation (and their sensing the space), if they lost it in spatial motions.

Summary: We studied, developed the orientation capabilities of our Hunveyor simulator, a planetary lander, on the Martian surface. By simulating we studied also orientation and space station activities for astronauts at the space station placed at the Lagrangian points of the Earth+Sun or Earth+Moon system.

References: [1] Bérczi Sz., Cech V., Hegyi S., Borbola T., Diósy T., Köllő Z., Tóth Sz. (1998): *LPSC XXIX*, #1267, LPI Houston; [2] Sz. Bérczi, T. Diósy, Sz. Tóth, S. Hegyi, Gy. Imrek, Zs. Kovács, V. Cech, E. Müller-Bodó, F. Roskó, L. Szentpétery, Gy. Hudoba (2002): *LPSC XXXIII*, #1496, LPI, Houston; [3] Duxbury, T.C., Kirk, R.L., Archinal, B.A., Neumann, G.A. (2002) Mars Geodesy/Cartography Working Group Recommendations. Symp. On Geospatial Theory, Processing and Applications. Ottawa, 2002; [4] Kabai, S., Bérczi Sz. (2001): *HyperSpace*, **10**. No. 2. 8.; [5] Kabai, S., Miyazaki, K., Bérczi Sz. (2002): *LPSC XXXIII* #1041, LPI.

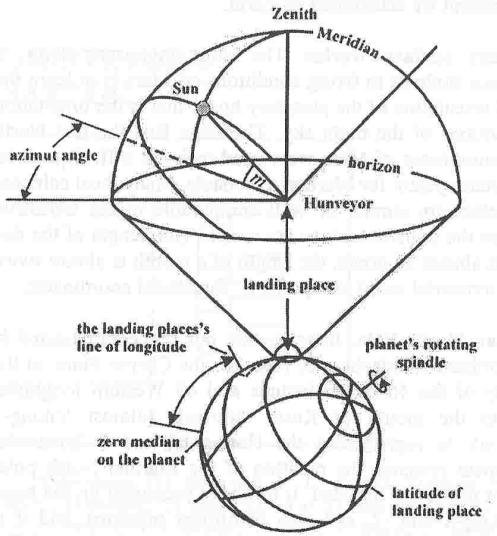

Fig. 1.2.4. The landed Hunveyor's frame of reference.

2.1. PROPOSED EUROPA ANALOG ICE-SPLITTING MEASUREMENTS AND EXPERIMENTS WITH ICE-HUNVEYOR ON THE FROZEN BALATON-LAKE, HUNGARY.

Introduction: Lake Balaton is a 70 km long and 8 km wide lake in Hungary. Its geological setting is in a tectonic fault. The lake consists of two basins: the NE one and the SW one. The average depth is 4 meters, but this depth does not exceed the 5 meters, except in one place, in the well of Tihany, where it deepens to 16 meters. The movements of the water inside the lake allows no regular modeling, because in case of the classical weave propagation model the amplitude of surface-weaves is comparable with the average depth of the lake.

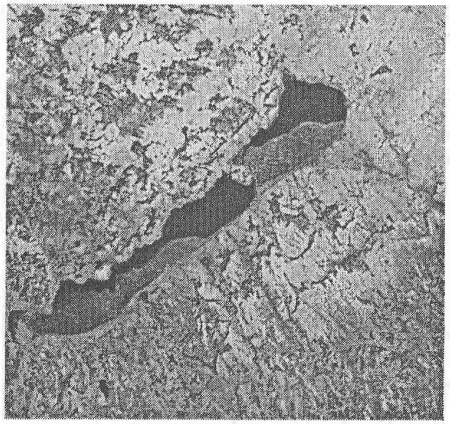

Fig. 2.1.1a and 2.1.1b. Lake Balaton in middle winter. The lake is partially frozen; the ice cover is lighter blue. NE of Tihany peninsula is the NE-basin, SW of it is the SW-basin of the lake (LANDSAT image [1]).

It is interesting that the average water level in the two basins may be different. The reason is that frequently, the SW winds push considerable amount of water into the NE basin lifting up that water level. When the wind ceases the response effect is that more water returns to the SW-basin, and then the average amount of water, therefore the local level there will be higher then resting level. This effect is a kind of balancing motion between the two basins which gradually relaxes. This mutually attached twofold alternating water system gives an extraordinary opportunity to study various effects of great water mass deformations. These possibilities are more exciting in wintertime when lake is covered by ice.

For example we may suppose that the motion of the Moon is affecting this amount of water, too. However, this tidal effect has not been yet measured because the average weaving – even during calm - overlaps this small effect. In winter, however, it is possible to measure the thin lifting/sinking effects on the top of the stable icy surface of Balaton Lake (Fig. 2.1.1.). We plan to connect these measure-ments with comparative planetary analogous effects, for example with those possible on Europa of Jupiter. The measurements are planned with Hunveyor university lander model. We call this experiment-assembly: Ice-Hunveyor.

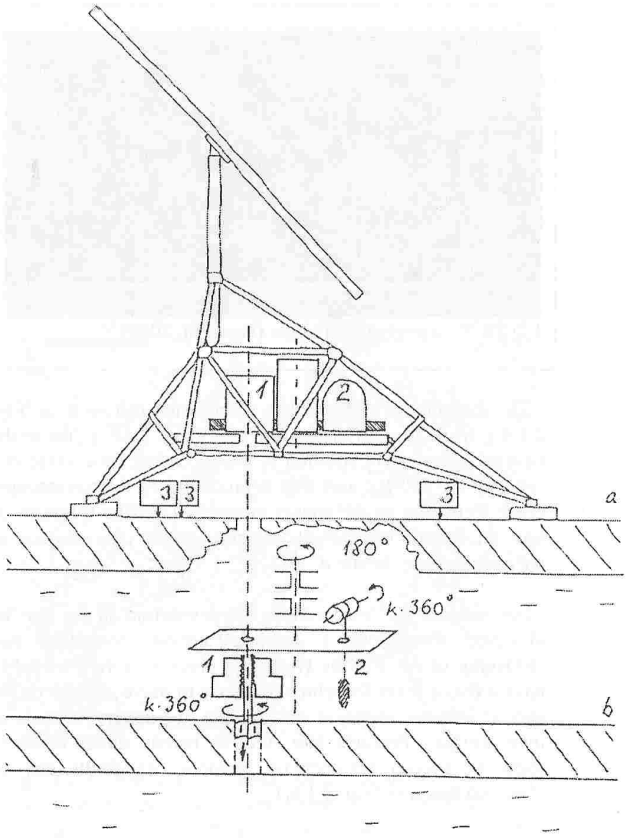

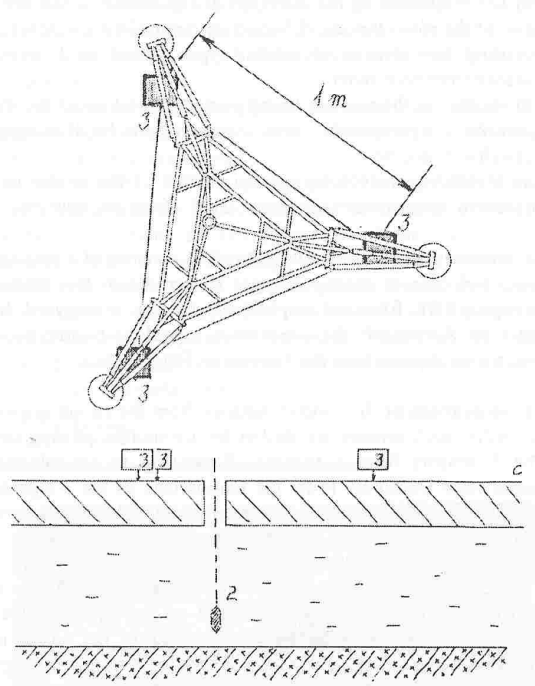

Fig. 2.1.2a and 2.1.2b. Ice-Hunveyor on the ice cover of Lake Balaton. On the instrumental platform the following elements can be found: 1: driller, 2: hydrophone with its rolling cylinder and 3: pick-up of sensors measuring ice-popping and fracturing in the sound frequency range (20 Hz - 20 kHz). Both 1 and 2 are placed on a rotating table which emplaces the hydrophone into the hole after a half turn rotation.

Fig. 2.1.2c. The measuring arrangement of the three sound frequency range sensors and the hydrophone hanged on. The triangular arrangement makes possible to determine the noise direction of popping and fracturing of ice from the phase differences of the arriving signals. Hydrophone measures the noise sources in water, mainly from biological motions (of fishes for example).

Special measurements on Ice-Hunveyor: The following four measurements are prepared on Ice-Hunveyor.

1) Measuring the self-noise of the ice in the sound frequency range (20 Hz - 20 kHz).

2) Determination of the direction of the source of the self-noise of the ice in the sound frequency range (20 Hz - 20 kHz) by using two sensors of similar types placed in 1 meter distance from each other.

3) Measuring the noise of living beings (fishes) under the ice cover by a hydrophone sensor hanged from Ice-Hunveyor through a drilled hole.

4) Measuring meteorological parameters of the winter environment: temperature: air, water; wind: direction, strength.

1. measurement: The main instrument consists of a pick-up (piezzo-electric or magnetic type) sensor. From this sensor through a FET, filter and amplifiers the signal is analyzed. In order to distinguish the ice-motion signals 3-6 amplitude levels were defined (one the 3 sensor of Fig. 2.1.2a.).

2. measurement: In 1 meter distance from the earlier sensor two other such sensors are settled for ice-motion picking-up. The 3 sensors form a triangle. Previously to ice-splitting noises were measured. From the comparison of the 3 signals the direction of the noise source are determined. (all 3 sensor of Fig. 2.1.2a. and Fig. 2.1.2c.). The 3 signals will have a phase-delay depending on their direction from source.

We determine the distance of the source by a fouth, a microphone detector which is hanged on the frame of Ice-Hunveyor in the air. (The arrival sequence of the noises is following: 1. is coming through ice, 2. is coming through water, 3. is coming from air. Earlier no such measurements of the propagation of cracking noises were made in all 3 phases – ice, water, air.)

3. measurement: The drilling is carried out in the symmetry axis of Hunveyor. The hydrophone gives the signal of noises from the water, which is compared with the signals from the surface sensors (Fig. 2.1.2b.) This noise of living beings should be extracted from the measured signals of surface sensors. Here we show some earlier results from meteorology.

Sonogram: The ice has a special sound that is being made in temperature change. This is the sound when cracks are being made, somewhat similar to earthquakes when stresses are released. The crack formation is most frequent in the moments of sunset and sunrise, i.e. in the terminator line.

Preliminary studies show that cracks has a sound sonogram similar to whistles made by the electromagnetic waves of lightning carried in the magnetosphere. Here the sound of cracks is carried in the ice.

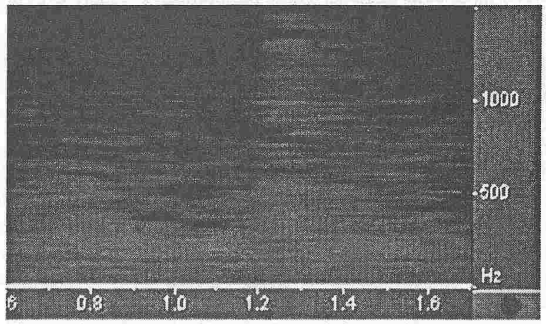

Fig 2.1.4. Sonogram from far (Hargitai, 2003).

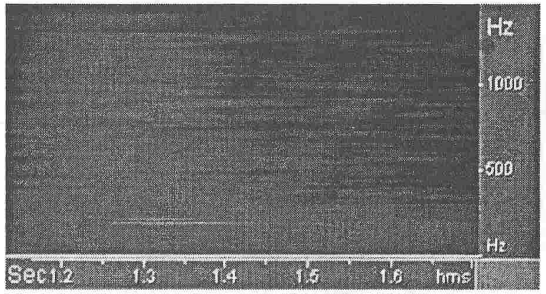

Fig 2.1.5. Sonogram from near (Hargitai, 2003).

The sound is only whistle-like when listened from a far (Fig. 2.1.4.), while it is different from near (Fig. 2.1.5.), like in the case of lightning. In addition to the ascending tone, there is a constant ca. 200 Hz tone that is produced by the microscopic crack formation in the sunset moments [3]. The question is: how the sound characteristic depends on the characteristic of ice and the water below it?

For microscopic observations, the evolution of ice can be observed throughout a seasonal period: formation and reddening of ice. For the Hunveyor probe it is very useful to have a Husar rover for which it is easy to move and search for special features otherwise inaccessible by humans (because of their weight). Features like Aeolian barcan dunes made of snow or special cryotectonic features like faults can be observed this way (Fig. 2.1.6.)

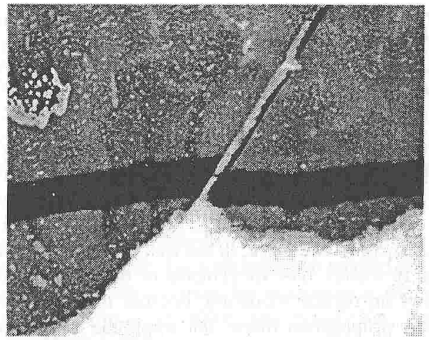
Fig. 2.1.6. Microsplitting before the large scale formation in ice. Length of the image is 20 centimeters (strike slip fault, photo by Hargitai, Dec., 2001).

The splitting cracks on Balaton Lake were earlier observed [3] and documented (Fig. 2.1.7.) by surface geodesic observations and aerial photography, respectively [4]. Since that no such survey was made, however it would be useful to find high resolution satellite images [1] for this task (although total freezing of the lake surface is a nonfrequent event).

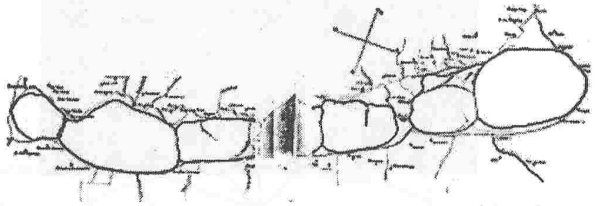
Fig. 2.1.7. Historical sketch about the large scale main splitting cracks on Balaton (Cholnoky, 1907) [3].

For planetary comparisons all the above mentioned can be used for the ice of Europa. We will investigate these in the winter seasons of 2005 and 2006 years, using the Hunveyor probe and its Husar rover.

References: [1] LANDSAT (1999): images of 188/27 and 188/28 taken on 1999-12-31. [2] Hargitai, H. (2003): Sonograms of ice-splitting at Lake Balaton, in winter of 2003/2004. [3] Cholnoky, J. (1907): *A Balaton jege.* (The Ice of the Balaton). [4] Budapest; Starosolszky Ö. (1984): A balatoni jég mértékadó terhelésének becslése. Budapest.

2.2. MEANDERING RIVERBED ANALOGS ON MARS AND EARTH.

Introduction: We made a hydrogeomorphologic comparison study between Martian ancient riverbeds in the Chryse Basin region and the main (recent and ancient) rivers - with Tisza as main river - of the Central Carpathian Basin. In the comparison meandering morphological characteristics were used according to four parameters: discharge, slope, rock and soil quality and planetary surface gravity. We concluded from this study that meandering characteristics of Martian river channels imply flowing water; while left-over river valleys or oxbow lakes show the longer history of flowing water in the studied area.

Chryse riverbeds: Many works dealt with flow rate of the Martian ancient rivers surrounding Chryse Basin [1], [2], and discussed similarities or analogies of the main rivers (Ares, Tiu, Simud, Shalbatana, Kasei) with some terrestrial counterparts [3]. Outflow channels on Mars once had extremely large water discharge [1], [2]. These studies investigated the upper, greater slope regions of these riverbeds. We now study the lower, slower, meandering region of Martian rivers. From meandering parameters not only flow rate can be estimated but also their historical development. For comparison we used Carpathian Basin rivers for terrestrial counterparts [4-6]. {The most meandering river on the Earth is Rio Jurua (Brasil), the largest of them is Mississippi, while the "most uniformly meandering river in Europe is Tisza River of Hungary" - as wrote Czaya in 1998. [7]}

Development of meandering riverbeds: The meandering rivers are in dynamic equilibrium in their capability of sediment transport and kinetic energy [8]. It does not deepens its bed or builds islands, but it meanders. The morphological characteristics of meanders are determined by 2 main groups of parameters: 1) connected to the energy of the river (water discharge, water velocity, the angle of the average slope of the terrain), and 2) connected to the materials of the riverbed soil/rock composition and homogeneity. In the case of homogenic bedrock the meander formation is ~uniform in the whole length of the river [6]; loose bedrock material or larger kinetic energy results in wider bends. A 3rd type of parameter in planetary comparisons is the value of surface gravity.

In addition to morphological characteristics of meanders, study of the cross section of river valleys can provide other data about the development of the river (i.e. terraces etc.) [1],[2], [9].

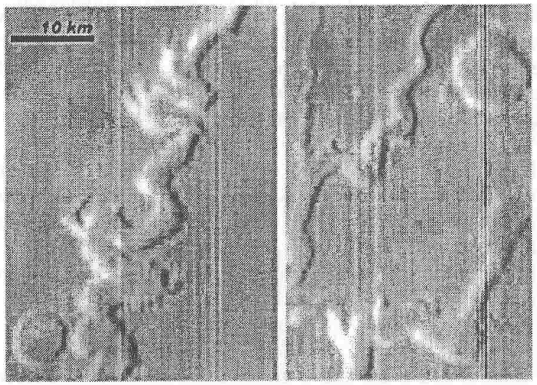

Fig. 2.2.1. Two segments of a meandering river valley of a smaller river on the Xanthe Terra at 6N 49W. MGS MOC m0305754 (ida.wr.usgs.gov) [10].

Ancient meanders of Tisza: The landscape development of the Great Hungarian Plain was determined by accretion of sedimentary layers by rivers during the last 1.5 - 2 M.y.s. On the 40000 km^2 surface the thickness of the river transported upfilling sedimentation is 500-1000 meters in average.

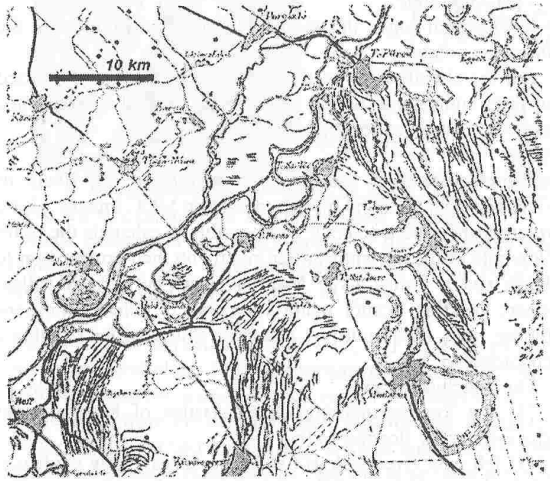

Fig. 2.2.2. Ancient riverbeds, dead channels and oxbow lakes following the Tisza river before its controlling in the Hortobágy region, Jász-Nagykun-Szolnok County, Hungary (map of Cholnoky from the XIXth C.).

The recent relief was modified on two greater regions in the basin by the winds, but the traces of ancient rivers and floods can be recognized on the 2/3 of the recent surface of the Great Hungarian Plain.

There is a maximum amplitude for meanders. When one meander reaches this size, it cuts off this bend, producing oxbow lakes or dry riverbeds.

In wet periods (like the springs in 1999 and 2000 years) there were extremely good conditions to determine ancient riverbed generations of Tisza, because of the visibility of ancient riverbeds and flooding. This extremely favorable visibility on satellite and air photographs means that even those riverbeds can be identified which has no any sign on the terrain. The color contrast of the ancient water-visited beds comes from the different water containing capacity of the layers below the surface soil.

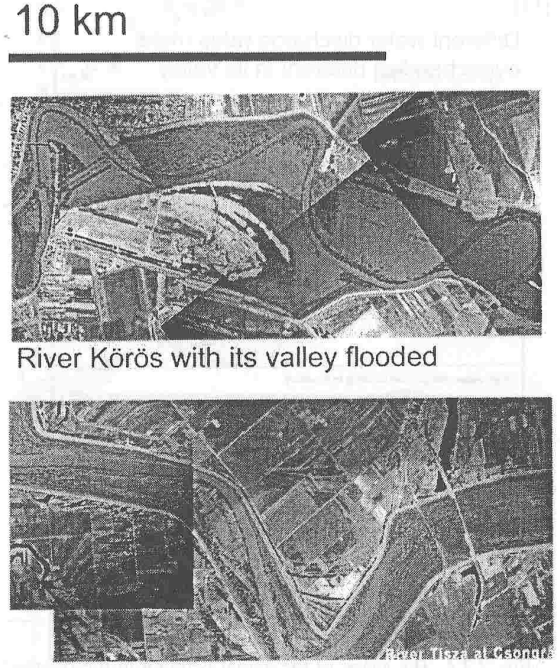

Fig. 2.2.3. Recent riverbeds of rivers Körös and Tisza.

Using these good observational possibilities we began to study the sedimentation, the morphology and accumulations phenomena of the river's ancient transporting and flooding

processes. On the basis of these observation we estimated the transporting capacity of ancient rivers (from as large rivers as Danube to as small as creeks) and their relative ages.

On Mars, recent high resolution MOC images [10] made it possible to investigate the smaller river channels (river beds), while on Viking images mainly river valleys are visible. For example in Nanendi Vallis the river channel is visible in the valley which support its origin by slow erosion of running water [11] (Carr 1999). On Mars in many cases ancient river beds has been obliterated by eolian processes (sand).

Paleohydrologic parameters can be calculated from the river beds and valleys morphological characteristics. Such calculation were made for outflow channels ([1] and [2] for Kasei Valles). In our investigation we use the bending (meandering) parameters (its degree of development) of two kinds of meandering: for valley meanders and free meanders [12].

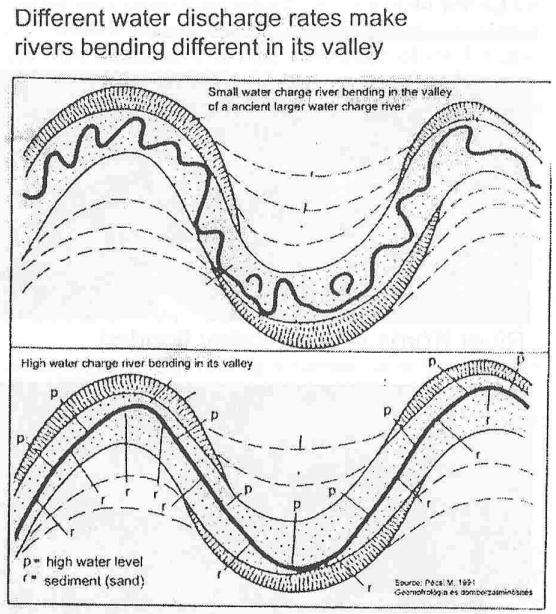

Fig. 2.2.4. The shape of the actual bending in the riverbeds follows the dynamics of the water discharge: in lower water (top) and in higher water (bottom) case.

We are also searching for other signs of meandering: old rivers beds, oxbow lakes, meander terraces. The bending parameters of old riverbeds can be used for paleohydrographic examinations which show the effect of climatic changes on rivers (for holocene rivers: [5]). Since the parameter of one bend depends on random variables, only statistical examination can provide accurate results, which give the average parameters for each different segment of the river.

Meander parameters of the development of ancient riverbed generations: Meandering geometry is in relation with the development of the water discharge of a river and with the slope of the terrain. Meander geometrical sizes (L: length of bend arc) and the water discharge (Q) are linked in the formula:

$$L = a\,Q^{b},$$

where a and b are and b are constant for a type of river meander and water discharge [1]. (Especially the arc length of a meandering between two inflexion points of a river's given meander is in proportional relation on a log/log diagram with the 10 % probability floods, for Tisza river [1], [2].) Such relations can be used for the estimation to the water discharge of a river if we now its meandering geometry.

In our study we compared river bends using the following parameters:

- (1) length of arc between inflexion points;
- (2) chord length (linear distance between inflexions);
- (3) Amplitude
- (4) central angle, the angle of the two radii normal to the inflexion points)

For the classification of the bends we used the classes used in Tisza controlling studies, where matured bend is determined as L=1,1-1,4 chord length, [13].

Conclusions and summary: Free meandering rivers or river beds can be found in high resolution MOC images. Using river meander parameters it was possible to calculate the water flow rate of the ancient Martian rivers, by their comparison to Earth rivers. (Most large Martian rivers cut off its valley, where bending occurs mainly because of relief conditions (crater rim), while outflow channels show a island building characteristic.)

Our conclusions are:

(1) the free meandering characteristics of Martian river channels imply flowing water;

(2) left-over river valleys (or oxbow lakes) show evidences of the longer history of flowing water in the given area. We continue our investigation in more detail. Ancient and recent bends of Tisza river proved to be a good counterpart for Martian meandering riverbed comparisons because their main hydrogeomorphological parameters are comparable.

References: [1] Mosangini, C, Komatsu, G. (1998): Geomorphology of Kasei Valles and scale of flooding episodes. *LPSC XXIX*. #1607; [2] Williams, R. M., Phillips, R. K. (1999): Flow Rates and duration within Kasei Valles, mars. *LPSC XXX*. #1417; [3] Costard, F., Gautier, E. (1998): Siberian rivers and Martian outflow channels: An analogy. *LPSC XXIX*. #1268; [4] Cholnoky J. (1907): Riverbed changes of Tisza. *Földr. Közl.* **35**. 381-405, and 425-445.; [5] Gábris Gy. (1986): Holocene water discharge of the rivers in the Great Hungarian Plain. (In Hungarian). In: *Alföldi Tanulmányok, 1986.* **X.** 35-51. Békéscsaba; [6] Lászlóffy W. (1949): A folyómedrek vándorlása. (The wondering riverbeds.) *Vízügyi Közl.* **31.** 98-116.; [7] Czaya E. (1998): *The rivers of the Earth.* Gondolat, Budapest; [8] Stelczer K., Csoma J. (1949): *Ármentesítés, árvízvédelem, folyószabályozás.* Tankönyvkiadó, Budapest; [9] Pécsi M. (1991). *Geomorphology and Relief Characterization.* (In Hungarian). MTA FKI, Budapest; [10] /ida.wr.usgs.gov/ ; [11] M. H. Carr (1999): Global History of Water and Climate. In the *5th Intl. Conference on Mars*, # 6030, [12] Kádár L. (1971): Specific types of Fluvial landforms related to the different manners of load transport. *Acta Geographica Debrecina. 1971.* [13] Laczay I. (1982): Morphological basis for plans of river regulations. *Vízügyi Közl.* **64**. 235-255.;

Appendix: Historical notes on controlling works of Tisza river in Hungary. There long traditions in Hungary to study the wandering of Tisza river and investigate ancient riverbeds because of the great number of floods of this river in the historical past. Especially the maps of the river made before 1830 (beginning of the controlling works) are extremely valuable. In the case of the Mississippi river experiments carried out on sand map between 1942-44 by the Mississippi River Commission are important counterparts. (W. Lászlóffy, 1949, [6]).

ANALYSIS OF THE MEANDERS OF SOME RUNOFF CHANNELS ON MARS

Introduction: The martian runoff valleys are thought to originate by sapping [1, 2, 3]. The exact style of the water flows, the sediment load, the discharge and many other factors are not fully understood [4, 5, 6]. The morphological and morphometrical results could help to resolve the circumstances of their origin, so it is an important field of work. In this article some part of the author's thesis [7] was summarized. The purpose of this is to show connections which possible can help in the future to understand the origin and evolution of these channels.

Working method: Based on the photos of the Viking-1 and –2 Orbiters [8] morphometrical parameters of the channels were measured by Surfer and Excel programs. The surveyed

area is between 0°-31°N and 44°-76°W. Beside the morphological characteristics the channels' width, length, and the amplitude, wavelength, radius of the meanders were measured. The error in most of the measurements is below 20%.

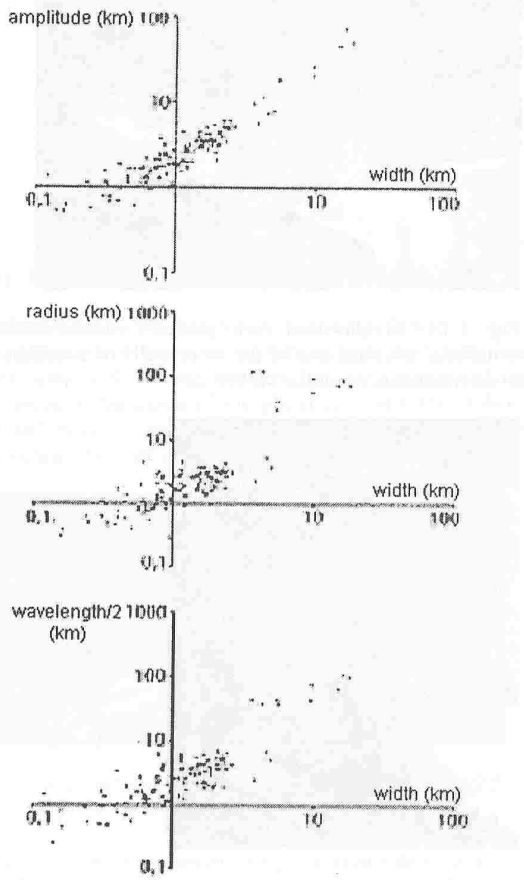

Fig. 2.2.5. Connection betweeen width and meanders' parameters

Results: At the runoff channels 110 meanders' amplitude, wavelength and radius were measured. Some well confined parts of the Kasei and Shalbatana valleys were also measured in spite that they are outflow channels with different origin [9, 10, 11, 12]. These parameters were indicated versus the width of the channels, which could be as a very rough approach of the relative discharge. There is good connection between the meanders' parameters and the valley width (Fig. 2.2.5.).

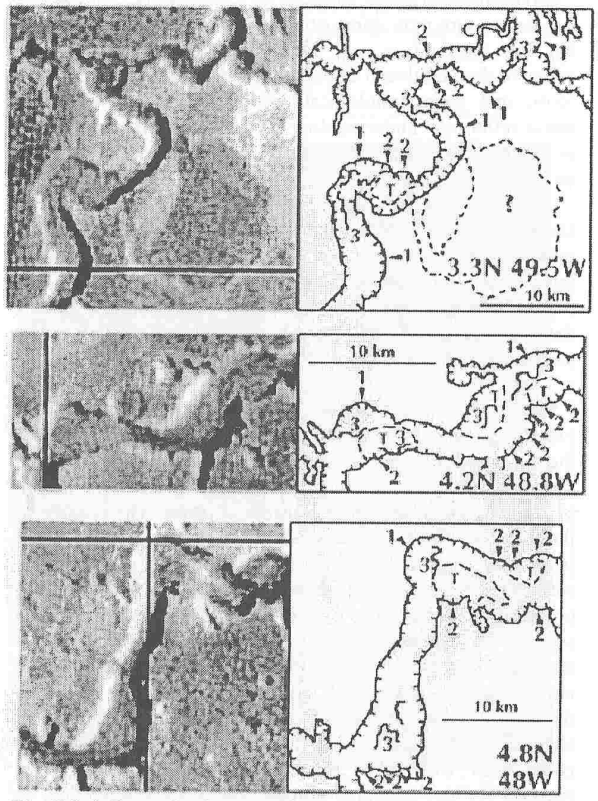

Fig. 2.2.6. Examples for several meander generations

Some parameters of the curvatures at the riverbanks were estimated as if they were meanders. Some of the results at three different channels are visible in Fig. 2.2.7.

On the Earth this relation is obvious, and there are methods in the paleohidrology [13] to estimate the ancient discharge with the meanders' parameters. Of course, on Mars the case is far different from the case on Earth, and the runoff channels are thought to formed by sapping. In spite this fact the upper mentioned possible rules may be real and arise from the inner physical characteristics of the moving water. (On Earth meandering style was observed at marine or atmospheric currents too beside the rivers.) So it is interesting to analyze these possible relations. The limited resolution of the Viking photos limited our work in the morphometric analysis.

At several runoff channels there are small but visible morphological characteristics which are possible results of moving meanders and variable discharges. In Fig. 2.2.6. are some morphological examples for the variable discharges at the same channel, as curving erosional structures at the riverbanks, small channel-like structures on the riverbed, and terrace-like structures (1,2,3 for traces of smaller and smaller meanders, and T for terraces).

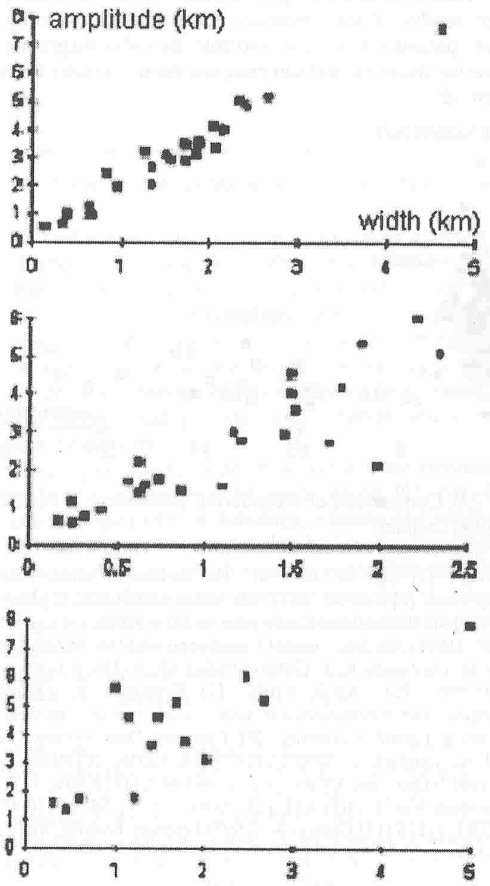

Fig. 2.2.7. Comparison of signs of ancient meanders (amplitude/width) at the same channels

If we indicate the amplitude/radius ratio versus the width at the first mentioned 110 runoff and 30 outflow meanders' parameters (Fig. 2.2.8.) the runoff and outflow channels are separated into two groups, where the outflows' meanders are less evolved and has always small amlitude. If the relations on Fig. 2.2.5. are real than it may help in the estimation of the paleodischarges of these channels.

Today there are many tophographic data from the MGS. With this data it is possible to estimate the the channels' cross section, and with the slope angle to estimate theoretical runoff speed. If these results are in good areement with the relative discharge results of the "meander method" than with the meanders' parameters we can estimate paleodischarges for many martian channles, and can compare them to results from other methods.

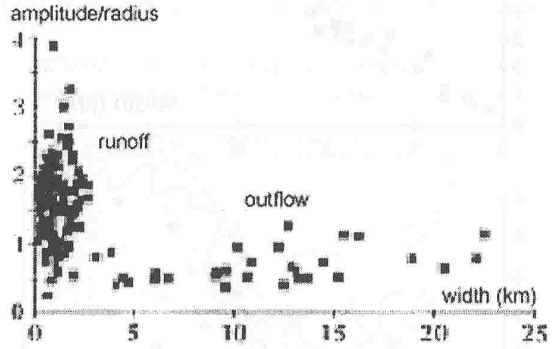

Fig. 2.2.8. Comparison of meandering parameters of runoff and outflow channels

References: [1] Carr M. H. 1981. The surface of Mars, Yale University Press, [2] Carr M. H. (1986) Icarus 65/187-202, [3] Carr M. H. (1999) 5th International Conference on Mars #6030. [4] Lee P., Rice J. W. (1999) 5th International Conference on Mars #6237. [5] Chapman M. G., Tanaka K. L. (2000) LPSC XXX. #1256, [6] Cabrol N. A. (1999) LPSC XXIX #1022, [7] Kereszturi A. (2000) Morphological and morphometrical analysis of martian channels, thesis, Eötvös Loránd University, [8] Planetary Data System [9] Skinner J. A., Tanaka K. L. (2000) LPSC XXX. #2076, [10] Baker V. R. et. al. (1987) Geol. Soc. Of Am. Vol. 2. 403-467, [11] Komar P. D. (1983) Geology Vol. 11. 651-654, [12] Kereszturi A., Sik A. (2000) LPSC XXXI, #1216 [13] Gábris Gy. (1995) Földrajzi Értesítõ, XLIV. 1-2, 101-109.

2.3. COMPARATIVE STUDY OF PERIGLACIAL MASS MOVEMENTS ON MARS AND EARTH

Intruduction By the methods of comparative planetology we can acquire new information not only from other planets, but from the Earth as well. The purpose of my research is to compare the periglacial environment of Mars and Earth, their forms and geomorphological processes. Hereby we might could refine our understanding of the paleoclimatic changes on these two planets and of the history of near-surface water on Mars.

I used the high resolution narrow angle images of Mars Global Surveyor's MOC [1] to define landforms and the profiles of Mars Oriber Laser Altimeter [2] to characterize the relief on the examined terrains. Because of the "difficulties" of real field work on the surface of Mars, I obtained these kind of data during a periglacial research expedition of my university, carried out in the summer of 2000.

Periglacial environment The periglacial regions most exactly can be defined by the termporary presence of ice under the surface. This often produce an ever-frozen, ice saturated section of the ground, called permafrost, which is the reason of the most periglacial mechanism and forms. The climate of these regions fluctuates round about 0°C in the year because it is needed to establish the conditions of ice-melting. The surface materials are also an important factor of the periglacial processes because most of these are related to rock debris covered surfaces. Well, it seems to be a complex environmental system and all these compounds are required to build-up a real periglacial landscape. Based on complexity these systems are very sentsitive to the smallest environmental changes and because of their dynamic character (in comparison with other morphoclimatological regions) the reaction for any changing comes very quickly after that. In addition, if the observed terrain has significant relief, the mass movements are particularly important.

Rock glaciers on Earth: As Earth-analogies, I collected data directly in two study area: 1. in a ruins of the former caldera of Erciyas Mountain in Anatolia, Turkey (38,5°N, 35,3°E) and 2. in a Northwest-facing valley in Aladaglar Mountains of Anatolia, Turkey (37,7°N, 35°E). These locations are approx. 3100 m above sea level. The results of this expedition are high scale topographic and geomorphologic maps, microclimatic measurements and a huge number of photograps.

At the first area (Fig. 2.3.1.) there are some middle-sized rock glaciers formed from the gravitational talus regions of the inner walls of the caldera. The most tipical form is a young and active, lobate-shaped rock glacier bordered by steep side- and front slopes and with well-defined transversal furrows-and-ridges pattern on its surface (Fig. 2.3.2.).

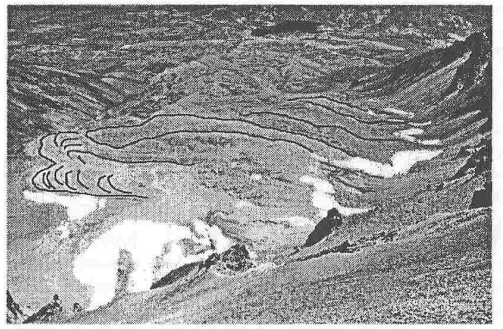

Fig. 2.3.1. Middle-sized rock glacier formed from the gravitational talus regions of the inner walls of a caldera in Erciyas Mountain, Anatolia, Turkey.

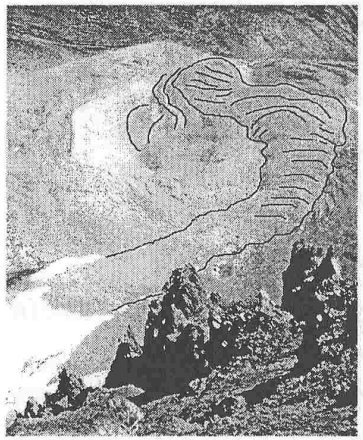

Fig. 2.3.2. Young and active, lobate-shaped rock glacier bordered by steep side- and front slopes in Erciyas Mountain, Anatolia, Turkey.

The second location is more isolated, in the Pleistocene it was a cirque-region of a normal glacier. Recently there is only one rock glacier in the area, so that can be very well bordered. The geomorpologocal map of this form (Fig. 2.3.3.) shows curvilinear pattern (similar that of Fig. 2.3.2.), as a result of

plastic deformation of inner ice-dominated layers. The lower end of this rock glacier has bigger units and deeper troughs between them. Perhaps it is resulted from changing active and less active (maybe inactive) periods of movement, in connection with variations of the environmental conditions.

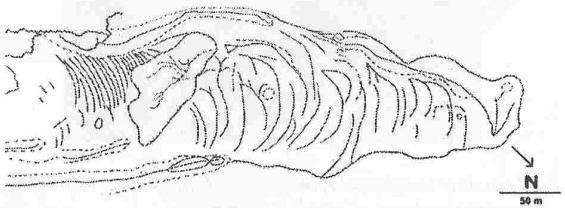

Fig. 2.3.3. Geomorpologocal ma pof the flow of Fig. 2.

Debris aprons on Mars: From Viking Orbiter images fretted terrains of Mars has known as high-relief transition zones between the young, northern low-lying plains and the old, southern highlands of the planet [3]. Here the isolated highland-mesas are surrounded by plastic, skirt-like forms of rock debris: these are called debris aprons (Fig. 2.3.4.).

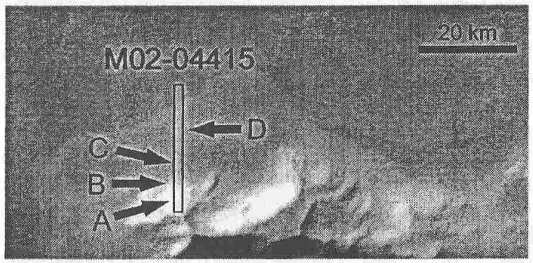

Fig. 2.3.4. Isolated highland-mesa on Mars, surrounded by plastic, skirt-like forms of rock debris. MGS image.

Their formation is supported by the existence of a global permafrost zone, called cryosphere, which was generated due to the atmosphere-loosing and cooling of the planet, when the surface water froze into the martian regolit [4]. Other morphological evidences of this latitude-specific ice-rich layer are the rampart craters, relief relaxation phenomena, poligon-shaped surface matrix, thermokarst-like features and indirectly the formation of outflow channels [5].

These debris aprons can extend to 15-25 km long, they have a convex shape, steep frontal- and side slopes and they are differs from gravitational talus or fluvial aprons, respectively. The source of their rock debris is the intensive physical weathering, and their ice emanates from the underlying layers, from the mesa's material or condense from the atmosphere [6]. Primarily the ice content-related mass movement mechanisms (continuous creep and episodic sliding) are responsible for the plastic appearance of these forms [7].

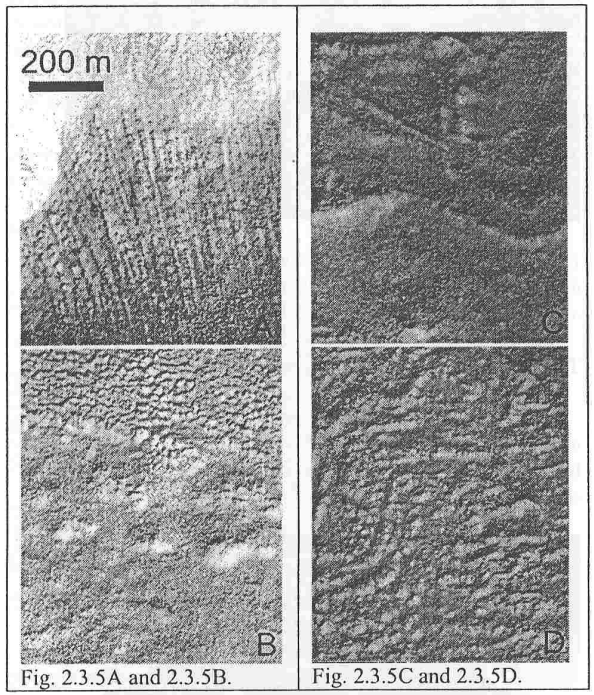

Fig. 2.3.5A and 2.3.5B. Fig. 2.3.5C and 2.3.5D.

Fig. 2.3.5. represent four high resolution details of MOC M02-04415 and Fig. 2.3.6. shows the matching MOLA profile of that MOC image. On 5A there is the source zone of rock debris, the weathering free rock face. On 5B there are tongue-shaped, sliding layer-units, like girlands on Earth. 5C illustrate a bigger mass movement, the curvilinear fronts of it (similar to drawings of Fig. 2.3.2.) are clearly visible. Finally, 5D is acquired at lower part of the apron and its morphology seems to be flatten again, according to the decreasing angle of slope.

Conclusions: On the basis of all the above mentioned things, truly the rock glaciers are the best terrestrial analogies of Martian periglacial debris aprons. They occur in similar environmental conditons, show analogous morphology and perhaps their movement mechanisms are the same as well.

The most important difference is the temporal variety of the periglacial environments of Mars and Earth, because our planet is more dynamic. For this reason, the same mechanisms acting on the two planets can resulted in different landscape, considering the importance of time of form-evolution [8].

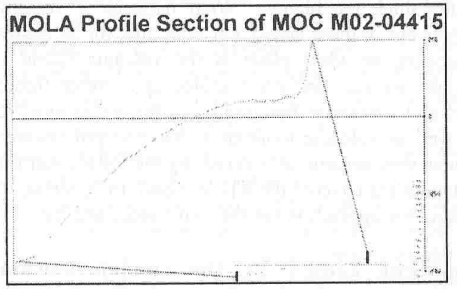

Fig. 2.3.6. MOLA profile of the mesa boundary of Fig. 4.

To find places from which there was taken a picture before and after 31st of August, 1999, I used Idrisi geoinformatic software. I tried just only some places and at these locations there is no sign of seasonal changes on the aprons. About longer period alteration we do not know any sure fact, because time expired since our first usable observations is very short. The detailed analysis of crater-density and crater erosion status might could provide more accurate time-information about these aprons.

We are planning to model these forms in the environment of our Hunveyor experimental space probe [9], but the best Earth-analogies (for its lithology, climate and orography as well) of these terrains are the McMurdo Dry Valleys of Antarctica [10], so new theories in connection with the topic of Martian periglacial environments there should be tested. By doing so, and by a better understanding of correlation between morphology of terrestrial rock glaciers and climatic oscillation, we will able to refine our view of near-surface water-history and paleoclimate of Mars.

References:[1] www.msss.com; [2] lptwww.gsfc.nasa.gov/tharsis/mola.html; [3] Squyres, S. W. et al. (1992) in Kieffer, H. H. et. al.: *Mars*, University of Arizona Press, Tucson, 523-554 [4]; Kereszturi, Á. and Sik, A. (2000) *LPSC XXXI*, #1216; [5] Carr, M. H. and Schaber, G. G. (1977) JGR, 82, 4039-4054; [6] Mangold, N. et. al. (2000) *LPSC XXXI*, #1131; [7] Vitek, J. D. (1987) in J. R. Giardino et. al.: *Rock glaciers*. Allen and Unwin, London, 239-264; [8] Humlum, O. (2000) *Geomorphology*. 35, 41-67; [9] Bérczi, Sz. et. al. (1999) *LPSC XXX*, #1332; [10] Nagy, B. and Szalai, Z.: Periglaciális lejtős tömegmozgások vizsgálata a King George-szigeten (Déli Shetland-szk., Ny-Antarktisz), *Földr. Értesítő*.

2.4. THE INTERACTION OF ICE AND VOLCANISM ON THE MARS AND IN ICELAND, EARTH.

The vast majority of the water supply of the Mars is present in a frozen state, partly in the regolith covering the surface, partly in the thick ice blanket. What happens if volcanic operation happens in these areas? For searching for an answer to this question, an ideal place is the volcanic island of Iceland, where we can find great analogies: extreme floods, maarcraters and volcanoes functioning in the widespread ice sheets, as well as volcanic mountains that emerged covered, but ever since they became uncovered by the ice blanket that at that particular era covered the whole island. In its strata, we can read about the interaction between volcanoes and ice.

Great outflows caused by the sudden volcanic melting of ice

The great territorial floods characteristic of the northern part of the Mars, called Chryse Platinia, although they were bigger, the circumstances of their creation could have been similar to the flooding of ice rivers in Iceland, called jökulhlaups.

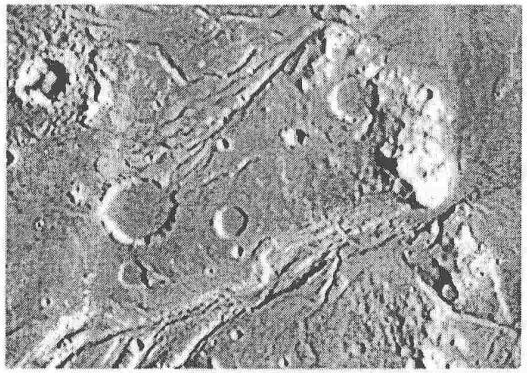

The Maya Valles (above), taken of traces of huge floods in the 10 kilometres wide, 1 kilometre deep and 180 kilometre long area of Vedra Valles (below).

The great thermic outburst gives life to a lake of melted ice, above which on average 200 m of ice blanket flows. In case of eruption, a huge quantity of ice melts and the great mass of water might break way to itself suddenly in the ice towards the ends of the ice sheet, from where it bursts as an extreme flood of outbreaking (200-300 m^3/sec), sweeping away icebergs and big rocks.

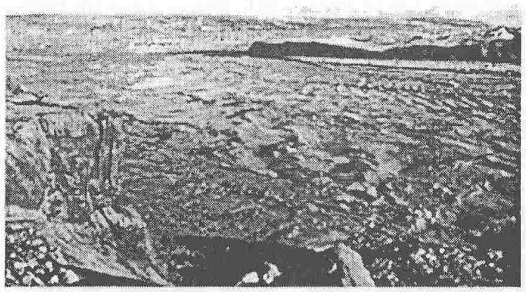

The greatest jökulhlaup of the last few years broke out in 1996 from ther Skeððarárjökull glacier of the ice sheet Vatnajökull, a few days after the eruption of Grimsvötn.

Table mountains (subglacial witness buttes)

Table montains (Tuya) are those ones that have emerged inside ice sheets and then, after the return of ice they have become well-separable, steep-sided mountains of regular shape.

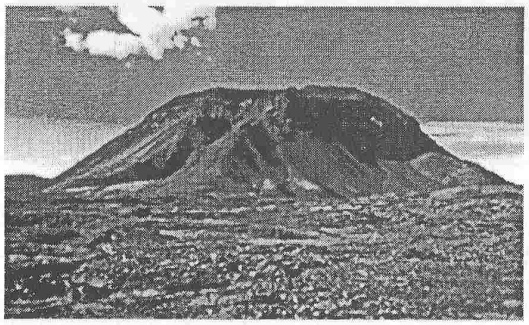

The Hlöðufell is a typical Icelandic witness butte of subglacial type, deriving from the upper-pleistocen.

Their upper, almost round-shaped plateau is in most cases a shield volcano. The diameter of its earthly representative is less than 10 kilometres, but they emerge by hundreds of metres from their surroundings. These shapes are to a great extent similar to those table mountains that can be found on the Mars.

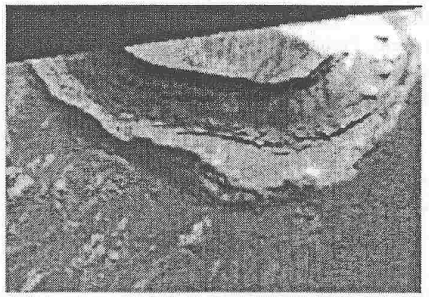

A possible subglacial table witness butte on the Mars, from the neighbourhood of Melas Chasma.

We can draw conclusions from how high the table mountains are about the thickness of ice blanket. In the initial period of the subglacial eruption, pillow lavas are being created. In a short period of time a lake consisting of melted water is formed, above which a few hundreds of metres high mass of ice can be found.

By the eruption continuing inside the ice, the building of pillow lava is getting higher and higher, while the highness of the ice and water strata will be smaller. At the same time an estuarine ditch, a cauldron is to be formed that is getting wider, while in the system of concentric circles the surface of ice is getting more fragmatic by crevasses. So the cauldrons are obvious signs of subglacial volcanic operation.

By the further thinnering of the ice strata, in the depth, along with the decrease of the water-ice pressure, the operation of the volcano inside the ice is changing to hyaloclastitic (hyaloclastite: volcanic shard deriving from sudden temperature decrease) tuff scattering (co-reaction of lava and water), while it breaks the ice. With the vastening of the tuff strata the vent is getting separated slowly from the intrusion of water, so the force of the explosions is getting less and less intensive, and after a certain period of time the volcanic operation is only characterised by flows of lava. These degassed, solidified flows of lava are protecting effectively the previous tuff stratas from any further external erosion in the future.

The strata of lava building up the table mountains are running down outwards from the vent, in a radial direction. On the shore of the once enclosing ice, the inclination to horizontal is quite frequent, and what is more, even the reassembling of it in the direction of the vent is just as often., that can be attributed to the reflooding impact of the enclosing wall of ice.

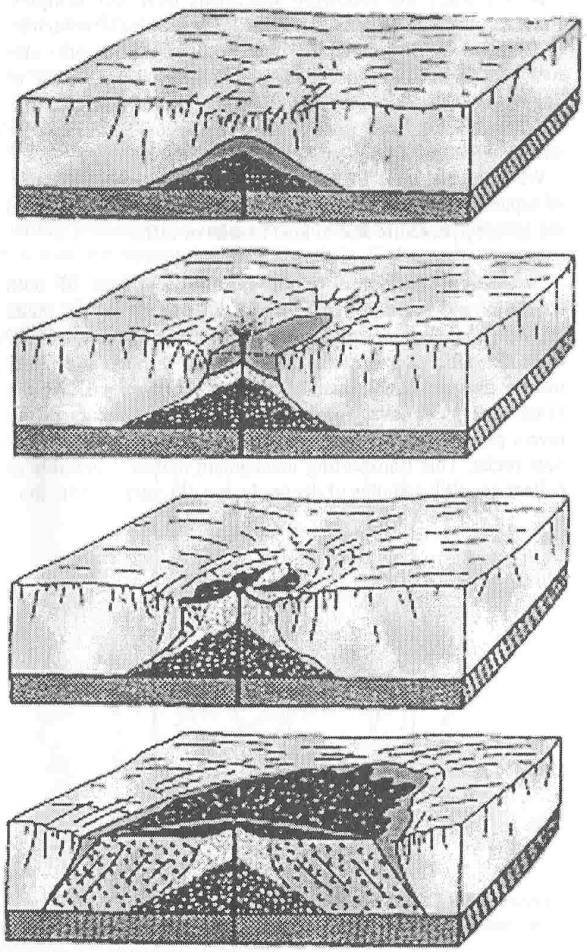

The creation of subglacial table-witness buttes

With the future regression of the ice sheet, the underposing of the gathered totality of tuff and lava realised by the ice had been cancelled, they will become unstable. As a consequence of this faultings, big falls and landslides are created. making huge wounds in the side of the volcanoe. The shard falling down makes a redeposed mass at the lower terrains of the mountain. Probably also those landslides can be of a similar origin that can be found at the side of the Olympus Mons.

„Chipped" shield volcanoes

Observing the steep, chasmic slopes of the Olympus Mons, it is highly probable that at these parts of the huge shield volcanoe's lavaflow confined by a thousands of metres thick ice sheet. So this huge volcanic mounatin is an „chipped" shield volcano, so it is a transitional shape type of the table mountains and of the shield volcanoes. Also for this we can find an excellent example in Iceland, the volcano, Legjabbrjótur, in the eastern side of the Langjökull ice sheet, one side of which is still covered by ice, the other part of it, the eastern one,which is 300-400 m high and chasmic is however already iceless, indicating the thickness of traces of the ice coverage once confined even the flows of lava.

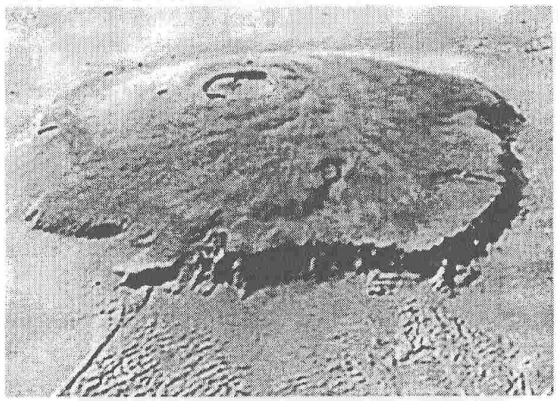

The gigantic lavaflows of the Olympus Mons would have been getting further in iceless environment.

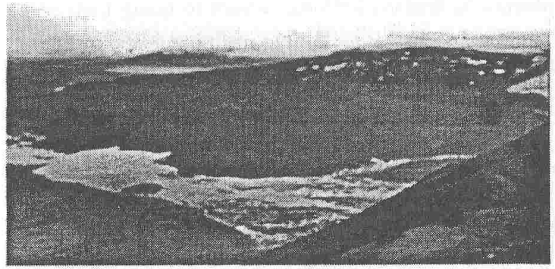

The Leggjabrjótur – on a smaller scale – is the best earthly analogy of Olympus Mons.

Rootless volcanic cones, maarvolcanoes

When the lava meets with wet soil, or stone, the groundwater can be heated by the great pressure. In this case, overpressurized water vapor is generated, and if this pressure of water steam is more than the pressure and the rip solidity of the coverage stones – in Iceland that of the lavas, on the Mars the regolith - it spreads explosively, while it smashes and brings with itself the surrounding stones (lava or regolith). The mixture of stones thrown out in the occasions of explosions falling back embraces around the shallow crater, that is eventually a pseudo-crater, because it does not feed itself directly from the magma chamber.

The diameter of the pseudocraters on the Mars and in Iceland is greatly depending on the subsurface water quantity and on the air pressure. The water content of the regolith covering the Mars is a lot less than that of which consists the environment of the Icelandic craters, but the sizes of the rings 5-6 times that of the Icelandics. This seemingly contradictory statement can be explained by the fact that the air pressure on the surface of Mars is much lower. That's why in Iceland 700-2000 kgs overheated water vapor are needed for a 20 m diameter ring, whereas on the Mars, on the Amazonis Planitia in order to build up a 100m ring the amount of 160-360 kgs water vapor are enough. Consequently, from the size of the maar rings on the Mars we can draw conclusions even about the frozen water content of the surface strata.

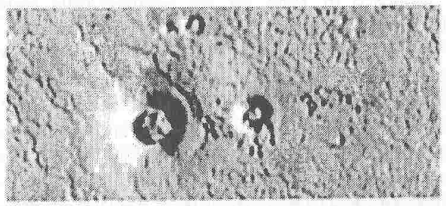

Possibly maar cones on the Amazonis Planitia

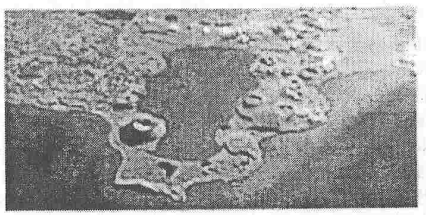

Pseudocraters on the shore of Lake Myvatn, Iceland

3.1. MARTIAN SHERGOTTITES AND THEIR COUNTERPARTS FROM THE SZENTBÉKKÁLLA SERIES OF MANTLE LHERZOLITE INCLUSIONS AND THE HOST BASALTS IN HUNGARY.

Introduction: Among the SNC (Shergotty, Nakhla and Chassigny) Martian meteorites there is a group which has several analogies with terrestrial basalt-with-xenolith rocks. These rocks are the shergottites. They form three main subgroups: the basaltic-shergottites (i.e. Shergotty itself), the picritic-shergottites or olivine-phyric shergottites (i.e. Northwest Africa 1068) and the lherzolitic or peridotitic shergottites (i.e. ALHA-77005. The three groups of shergottites has formation ages between 170 and 500 Mys.

Genetic and textural characteristics of the host basalt and some of its inclusions are analog from Szentbékkálla, North-Balaton Mountains, Hungary, to the range of the shergottites. Here several types of peridotitic rocks (lherzolites, websteries and harzburgites) can be found as inculsions int he basalt of tuff and the olivine-phyric basalts also can be found among the basalts of the Little Hungarian Plain and Tapolca Basin.

Model for origin of shergottites: Considering geochemistry of shergottites Warren and Bridges [1]. suggested a classification to the three subgroups. In this model degree of assimilation of the crust components distincts those magmas coming from martian mantle. This model is similar to that we proposed in 1984 for the Szentbékkálla series of inclusions. When the martian basaltic partial melts leave their source regions they exhaust it in some geochemical components, mainly REEs. According to the exhausting level they defined strongly (S), median (M) and lightly (L) exhausted shergottites. The S-shergottites are represented by QUE94201, the M-shergottites are by ALHA77005, and the L-shergottites by Shergotty and Zagami. (Although the L-shergottites can be also be derived from the S-shergottites so, that the uprising lava assimilated crust components with large REE content.)

Suggested source regions for olivine-phyric shergottites: The MER rovers discovered that a shergottite type may exist int he form of surface boulders along the tripway of Spirit in Gusev crater. McSween reported on the 36th LPSC that the olivine rich Martian basalts may be the counterparts of the olivine-phyric shergotties on the basis of the Pancam textural images, the miniTES and Mössbauer spectrometer data [2]. The olivines (phenocrysts) occur in visible sized porphyric form as (25 %) textural component of rocks Humphrey, Adirondack, and Mazatzal in the Gusev-crater. The Fe/Mg ratio of these olivines were also similar to that of olivin-phyric shergottites. Because of the spectral similarities of these rocks to the southern terra rocks on Mars, Spirit MER Team suggested that mainly such a basalt, the olivine-phyric shergottite forms the Noachian terra. According to Irving et al. (2005) the Tharsis volcano mountains are the sources of the olivine-phyric basalts.

The Szentbékkálla series: Several basalt volcanic units in the North-Balaton Mountains, in the Little Hungarian Plain and other parts of the Carpathian Basin (Nógrád-Gömör Mts, Persány Mountains in Transylvania, Romania) contains mantle xenoliths. We selected the Szentbékkálla locality as example counterparts for shergottites. Mantle xenoliths were collected and studied from the Szentbékkálla basalt tuff and also from other basalts and tuffs of the North-Balaton Mountains region [3]. Mantle xenoliths specimens, however, from Kapolcs, Szigliget, and Sitke were also studied.

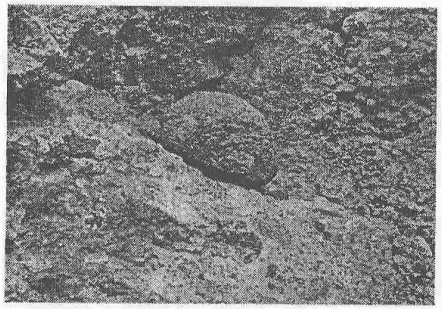

Fig. 3.1.1. The basalt tuff with ultramafic inclusions and a fist sized lherzolite xenolith separated from the basalt, from Szentbékkálla, North-Balaton region, Hungary.

Two types of lherzolites are the main ultramafic inclusion types in Szentbékkálla: exhausted lherzolites with smaller grains size and protogranular lherzolites with lightly exhausted REE content. The first group is more harzburgitic in mineral composition because olivine and orthopyroxene are their main mineral constituents. The second – protogranular – group is composed of the four main mineral phases of the lherolites: olivine, orthopyroxene, clinopyroxene and spinell. The exhausted lherzolites group is a good petrographic analog to the peridotitic-(lherzolitic)-shergottites, because they are similar to these harzburgitic-lherzolitic rocks. The series contains basalts with large olivine xenocrysts, too. These rocks are good mineralogical counterparts of the olivine-phyric shergottites also containing large olivin xenocrysts.

In this study the following specimens were our **samples**: Progran, Average-Lehrzolite, Wehrlite and Spinel-pyroxenite. (A Dunite and a Layered-Lherzolite sample were also included from the xenoliths.) The host basalt samples of Szentbékkálla, Szigliget and Kapolcs were also studied. INAA, electron microprobe and petrographic microscopic studies were carried out ont he samples.

We measured the REE content of the various xenolith types, of separated mineral components of the average lherzolite and the spinel-pyroxenite and of host basalts or tuffs.

Discussion: Peridotite is the basic component of both terrestrial and Martian mantle. From this mantle partial melts are separated and pour on the surface or crystalize in the upper crust. Basaltic or picritic lavas penetrate through the upper mantle and crust and assimilate some components. At the same time these lavas may convey broken fragments of the layers penetrated and they are embedded as xenoliths in the host rocks. This transporting mechanism makes it possible to collect xenoltih samples of deeper layers of upper mantle, too.

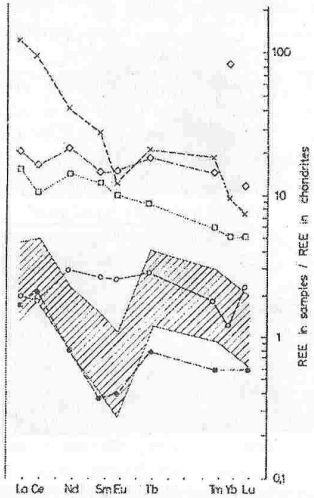

Fig. 3.1.2. Chondrite normalised REE abundances in the members of the Szentbékkálla ultramafic inclusions. X – basalt, ⟨ – wehrlite, □ – spinel-pyroxenite, ● – dunite, ○ – layered lherzolite.

The various xenolith represent different formation mechanisms. On the basis of mineral composition and REE abundance pattern it is possible to sketch the formation history of various xenoliths. On the basis of such measurements the petrologic genetics of the Progran, the Average-Lehrzolite, the

Wehrlite, the Spinel-pyroxenite (and the Dunite and the Layered-Lherzolite sample) were derived. Three factors have affected the REE abundances of these ultramafic inclusions. These factors are: partial melting from the mantle source, partial sparation of the melted liquids from the source environment and assimilation on their way from mantle source to the surface.

REE almost totally partition into the melt during the partial melting process. The high REE concentrations originated in this way are transported with the melt. If the melt separates from the source region, moves away and crystallizes, the degree of partial melting is inversely related to the degree of partial melting [4].

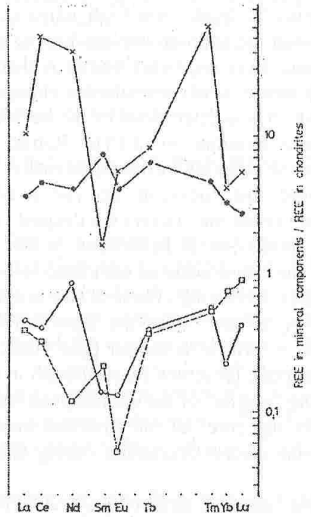

Fig. 3.1.3. Chondrite normalised REE abundances of the 4 mineral separates of average lherzolite from Szentbékkálla. X – spinel, • – diopside, o – olivine, □ – enstatite.

But melt rarely separates totally from its parental environment. In localities, where it had been retained, the REE concentration increased. On the whole parental region the REE concentration decreased exhausting the source region both in main minerals of partial melting, and REE elements. In localities, here partial melts crystallized, the host rock has elevated REE concentration. Finally, assimilation of components from the penetrated rocks may also change liquid composition [5].

The Szentbékkálla series of ultramafic inculsions can be arranged according to these processes. The highest REE abundances characterize those samples which has originated by separation of the melt from the parental environment. Both basalt lavas poured onto surface and Spinel-pyroxenite samples crystallized in depths has such high REE abundances. The second group of samples consists of xenoliths which retained more (i.e. Layered lherzolites) or less (Wehrlite) of their lherzolitic composition in spite of the fact that more partial melts had accumulated – and later crystallized – in them, as compred those which had separated from them partially.

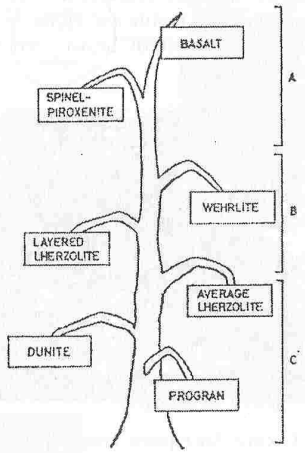

Fig. 3.1.4. Arrangement of the Szentbékkálla series of ultramafic inculsions according to separation of the melt from the parental environment, enrichment and exhausted nature of their REE abundances [3].

The third group of mantle xenoliths consists of lehrzolitic inclusions which in some degree has depleted in components (as REE) which had gone into partial melts. The Average lherzolite, the Dunite sample may belong to this group. Probably the Progran sample is the less exhausted one among xenolith inclusions of Szentbékkálla.

References: [1] Warren, P. H., Bridges, J. C. (2005): Geochemical Subclassification of Shergottites and the Crustal Assimilation Model. *36th LPSC*, #2098. LPI, Houston; [2] McSween, H. Y., Jr., Milam, K. A. (2005): Comparison of Olivine-rich Martian Basalts and Olivine-Phyric Shergottites. *36th LPSC*, #1202. LPI, Houston; [3] Bérczi Sz., Bérczi J. (1986): REE Content in the Szentbékkálla Series of Peridotite Inclusions. *Acta Mineralogica et Petrologica Szeged.* **XXVIII**. p.61-74, [4] Ringwood, A. E. (1975): Some aspects of the minor element chemistry of lunar mare basalts. *The Moon*. **12.** 127-157. [5] Bérczi Sz. (1991): *Kristályoktól Bolygótestekig*. 210.old. Akadémiai Kiadó, Budapest.

3.2. TERRESTRIAL IMPACT MELT ROCK AND BRECCIA FROM THE MIEN CRATER, RAMSÖ ISLAND CENTRAL PEAK, SWEDEN.

Introduction: The vesicular, "rhyolitic" sharp pebbles from the Ramsö Island, Mien Lake, Blekinge County, Sweden represent terrestrial impact melts and breccias, because the Mien Crater has impact origin and the central peak is the Ramsö Island. The impact melt rocks from Ramsö Island earlier were classified as rhyolites. In our samples it can be observed how impact melting transformed and preserved some parts of the original texture.

At the beginning of XXth century the first two ring shaped geological structures identified as astroblemes (with exogenic impact origin) were: the Barringer Meteor Crater in Arizona, United States, and the Siljan ring shaped (lake and mountain) structure in Dalarna Region, Sweden. Till the end of the 80-es more than twenty candidates to astroblemic structures were found in Sweden [1] and more than thirty in North America [2] and about a hundred all over the world [2]. There are more then 10 very probable Swedish astrobleme structures. Mien Crater is the southernmost one, and can be found in Blekinge Region, about 30 km from the Baltic Sea shoreline.

Historical background: Mien Crater has got its name from the lake Mien, which occupies a circular depression. This depression had been excavated into the Precambrian gneiss-granitic bedrock in the Cretaceous Period [1]. Holst [3] found (in 1890) boulders scattered around the lake, but mainly in the lake's northern vicinity. In his field and microscopy observations he supposed volcanic origin for these special rocks and he sent samples to Gy. Szádeczky (Hungary), and Zirkel (Germany) to study them. Gy. Szádeczky had earlier studied Hungarian rhyolites, especially from the Vlegyásza-Bihar Mountains [4]. Szádeczky found many similarities between Swedish and Hungarian rhyolites [5]. Holst [3] had also described them as rhyolites and that was the accepted classification of Mien-rhyolites till the work of Svensson and Wickman [6] who identified coesite (the shock-metamorphic variety of quartz) in the Mien-rhyolites, and so first they proved the impact origin of the Mien Crater [7]. Finally, test drillings proved, that the rhyolites, which were found earlier only as boulders (glacial deposits), could be found below a moraine layer (3-5 meters) and formed a 20-25 meters thick layer of bedrock of Ramsö Island, the central peak of the Mien Crater [7].

Geomorphology of the Mien astrobleme: The mountain ring which encircles the Mien Lake depression, has about 5 kilometers in diameter. It has a very special impact-geological characteristic: it has a central peak which emerges in the NW central part of the lake, as an island, the Ramsö Island.

The impact, which formed the Mien Crater, excavated the gneiss-granitic bedrock [1]. Crater formation models agree, that impact melt can be produced in the central depression. This impact melt forms a thin cover in the central region of the crater depression, and solidifies as volcanic rock and breccia. Central peak uplift had broken this impact-melt-cover and became the Ramsö Island. The northwestern shoreline of Ramsö is densely populated by "rhyolite" blocks. These broken blocks were transported and scattered as glacial deposits in the form of boulders on the northern and western shorelines of the lake [7].

Description of the samples:

Macroscopic study The Mien Crater samples from Ramsö Island are mainly in the form of "sharp-pebbles", rounded by the water erosion. Their surface therefore, frequently exhibit a clear cut cross section of the rock, and so show the texture in naked-eye visible scale. This visible texture consists of light and light pink and yellow fragments and larger inclusions, sometimes granitic inclusions, and more or less vesiculas (bubbles) embedded into a lighter or darker gray mesostasis. Mesostasis seems to be homogeneous on this scale. Larger (two-three fist sized) specimens contain inclusions of some centimeter sized fragments, too. The western shoreline of Ramsö Island is populated almost exclusively with such samples.

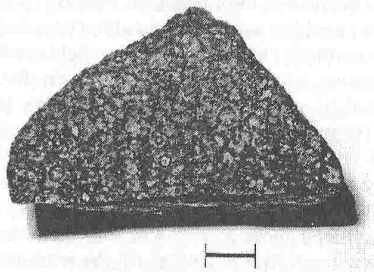

Fig. 3.2.1. Sharp pebble, brecciated rock specimen from the Ramsö-Island, Mien-crater central peak, Sweden.

Microscopic study Two samples were chosen for microscopic observations. Both samples show some kind of complexity which means that most of the samples can be identified as "impactite" with variolitic texture, but we could observe parts with higher proportion of glass and smaller potash feldspar crystals with intersertal texture and also some parts with brecciated texture. Brecciated parts contains several minaral fragments of the preimpact rock (Fig. 3.2.1.). The rock is rich in small unfilled vesicles, too.

Both samples contain potash feldspar, quartz, plagioclase, glass, opaque minerals (sometimes tiny grains of translucent ilmenite can be observed), rutile, hematite, limonite. Tiny biotite crystals were identified in the microprobe investigations, but in microscopic observations we could find only pseudomorphs after biotite and probably after amphibole. The pseudomorphs consist of brown, reddish brown, fine grained limonite, hematite.

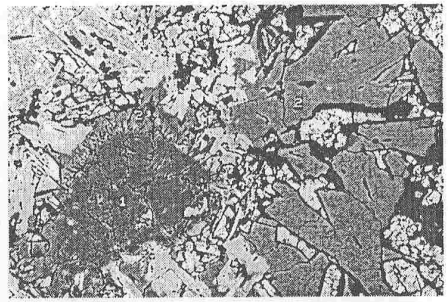

Fig. 3.2.2. Electron Microprobe image of Ramsö breccia. Relict quartz grain is surrounded by feldspar laths. (image width is 500 μm)

Potash feldspar (sanidine?) laths or fibers mostly show radiant or divergent arrangement (Fig. 3.2.2.) which prove quite rapid cooling of the molten material in the variolitic parts. The intersertal parts are characterized with unoriented potash feldspars with polygonal interstices occupied by glass (with composition close to that of the potash feldspar according to reconnaissance microprobe analyses), microcrystalline quartz and ilmenite.

Quartz seems to be mostly a relict phase, it forms rounded polycrystalline aggregates with glass rim and clear indication of resorption on the edge of the aggregate. The composition of the glass rim is close to that of the potash feldspar (Fig. 2.). The boundary between the individual quartz grains in the aggregates is sutured. It seems from these textural features that the quartz aggregates suffered some kind of recrystallization. The aggregates of quartz are full of tiny opaque minerals, possibly ilmenite and with reddish hematite. New microcrystals of quartz crystallized from the melt can be found mainly in the intersertal parts, in the interstices of the potash feldspar associated with glass (potash feldspar glass) and ilmenite. Both quartz and potash feldspar are highly strained having undulating extinction.

Relict plagioclases of the preimpact rock are rarely observable in the parts having intersertal texture and in the brecciated parts.

The brecciated parts are bordered with plagioclase showing radiant arrangement and multiple twinning, glass and sometimes biotite. The breccias contain major strained quartz, plagioclase. microcline and accessory biotite, muscovite, amphibole, zoisite and zircon clasts in fine grained brownish groundmass.

Summary, conclusions: The Cretaceous impact which excavated the Mien Crater, had melted some parts of the gneiss-granitic bedrock. The high silica containing granitic composition of the bedrock implies that the impact melt was a rhyolithic one. (The impacting body could add only some few percents to the melt, but it could not change the character of the melt, which was determined by the bedrock chemistry, and the sediments stratified on it.).The Ramsö Island "rhyolite" samples are the rocks of the solidified melt.

How could this rock-unit become available on Ramsö Island? The impact melt covers the deepest central parts of the excavated depression. Solidification of this impact melt is a process of short time scale as compared to the long time scale (10000 years) of relaxing effects of stressed bedrocks below it. This relaxing effects couse the slow uplift of the stressed bedrocks in a form of a central peak "needle" of the crater. The central peak preserves its stratification during the uplift, therefore the "needle" of the central peak represents a kind of a "large drilling core" of the stratified materials, which had layered in the central depression during and after the impact event.

Above this "needle", surface layers could be moved (eroded) away by glacial movements on that region (proved by moraines recognized). Underlain to this moraine layer the impact-melt-originated rhyolite layer lies, together with some breccias also of impact origin. Later erosion modified the broken fragments of this 20-25 meters thick layer, and this was the case in glacial period, when "sharp-pebble" shape of the broken rock samples was formed by eolic erosion.

In conclusion: Ramsö Island (Mien Crater's central peak) fragments

1) are impact melts with vesicular structure,

2) have "sharp-pebble" shape by eolic erosion,

3) later were weakly rounded by the water erosion in the lake.

References: [1] Wickman, F. E. (1988): Possible Impact Structures in Sweden. (In: *Deep Drilling in Crystalline Bedrock*. Vol. 1. Bodin, A., Eriksson, K. G. Editors.) Springer Verlag, Berlin; [2] Grieve, R. A. F. (1982): The Record of Impacts on Earth: Implications for a Major Cretaceous/Tertiary Impact Event. (In: *Geological Implications of Impacts of Large Asteroids and Comets on the Earth*. Silver, L.T., Schultz, P.H. Editors.) Geol. Soc. of America. Spec. Paper No. 190. Boulder, Colorado; [3] Holst, N. O. (1890): *Ryoliten vid sjön Mien. Sveriges Geologiska Undersökning.* Ser. C. No. 110. Stockholm; [4] Szádeczky Gy. (1904): Adatok a Vlegyásza-Biharhegység geologiájához. (Data to the Geology of the Vlegyásza-Bihar Mountains.) *Földtani Közlöny*. **34.** pp. 2-63. (and in German: Beiträge zur Geologie des Vlegyásza-Bihargebirges. *Földtani Közlöny*. **34**. pp. 115-184.) Magyarhoni Földtani Társulat, Budapest; [5] Szádeczky Gy. (1888): Rhyolithnyomok Svédországban. (Rhyolite traces in Sweden) *Földtani Közlöny*. **19**. pp. 395-406. (and in German: Rhyolithspuren in Schweden. *Földtani Közlöny*. **19**. pp. 437-449.) Magyarhoni Földtani Társulat, Budapest; [6] Svensson, N. B., Wickman, F. E. (1965): Coesite from Lake Mien, Southern Sweden. *Nature*. **205**. No. 4977. 1202-1203.; [7] Stanfors, R. (1969): Lake Mien - an Astrobleme or a Volcano-Tectonic structure. Geologiska Föreningens: Stockholm Förhandlingar, GFF. 91. pp. 73-86. Lund;

3.3. IMPACT MATERIALS OF THE RIES CRATER, GERMANY.

The Nördlinger Ries is a complex impact crater, which is located in the Southern Germany (N 48°53', E 10°37') with a rim-to-rim diameter of about 26 km (Engelhardt, 1990; Deutsch, 1998). Its excellently preserved ejecta blanket and breccia lens offer one of the most remarkable conditions for studies of impact cratering record and its geological consequences on Earth (Engelhardt, 1990) (Fig. 3.3.1). The 15 Ma age of the Ries crater was determined by ^{40}Ar-^{39}Ar method using rocks and impact glasses (Staudacher et al., 1982).

Geological summary of the Ries impact crater: The preimpact stratigraphy of the target rocks contains a crystalline basement of pre-variscian gneisses and amphibolites and variscian granite. These crystalline rocks were covered by sedimentary rocks of Upper Jurassic (limestone), Middle Jurassic (sandstone, marlstone, limestone), Lower Jurassic (sandstone, marlstone, limestone), Upper and Keuper (sandstone, siltstone, marlstone, claystone) and Lower Triassic sandstone. The southern part of the present basin was covered by ~25 m of unconsolidated Upper Miocene sands, marls and clays (Engelhardt, 1990).

Ries impact materials: The *so called* Bunte Breccia is an approximately 600 m thick ejecta deposit (representing an asymmetric present distribution) composing unshocked and moderately shocked rock and mineral fragments of sedimentary and crystalline megablocks and monomict breccias (derived from the crystalline basement) (Deutsch, 1998).

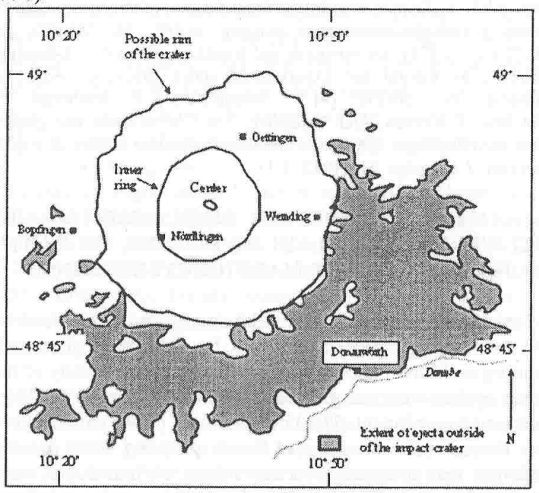

Fig. 3.3.1. Geographical map of the Ries imapct structure representing the location of the ejecta blanket (after Engelhardt, 1990)

The presence of shatter cones indicates that these rocks were affected by low shock pressures belonging to the low peak shock level (<10 GPa) (Engelhardt, 1990). The high peak shock level effects (>10 GPa) on quartz and other rock forming minerals (e.g., plagioclase feldspar) such as planar deformation features (PDFs) were described from shocked granite inclusion in suevite (Engelhardt and Stöffler, 1965) (Fig. 3.3.2).

Fig. 3.3.2. Multiple sets of PDFs developed in a quartz grain from a shocked granite inclusion in suevite from the Ries Crater (Germany). Note the irregular extinction within the quartz grain (from French, 1998.).

The other shock metamorphic indicators such as high-pressure mineral phases (e.g., coesite, stishovite) (Stöffler, 1972), diaplectic glass (e.g., feldspar transformed to maskelynite) (Stöffler, 1966) and fused quartz glass (lechatelierite) (French, 1998) from suevite were also found in the Ries Crater (Fig. 3.3.3.).

Stage	Shock effects	Pressure (GPa)	Post-shock Temp. (°C)
0	Fragmentation; mosaicism;undulatory extinction; deformation bands in quartz; kinkbands in biotite; shatter cones	0-10	0-100
I	Planar elements in quartz; planar deformation lamellae in feldspar, amphibole and pyroxene; stishovite, coesite; kink bands in biotite	10-35	100-300
II	Diaplectic glasses of quartz and feldspar; deformation lamellae in amphibole and pyroxene; kinkbands in biotites	35-45	300-900
III	Selectively fused feldspar; diaplectic quartz glass; thermal decomposition of biotite and amphibole	45-50	900-1300
IV	Complete fusion of rocks (granitic composition); impact melts	60-80	1500-3000
V	Vaporization	>80	>3000

Table 3.3.1. Stages of shock metamorphism in the Ries impact structure (from Engelhardt 1990).

The Ries Crater has been known as a source crater of moldavite tektites (Central European Strewn Field). Recently, Boggs et al. (2001) identified planar deformation features (PDFs) in shocked quartz from the Ries Crater, Germany using the scanning cathodoluminescence imaging facility and discussed some differences between these shocked quartz grains and planar microstructures in quartz associated with tectonic fracturing.

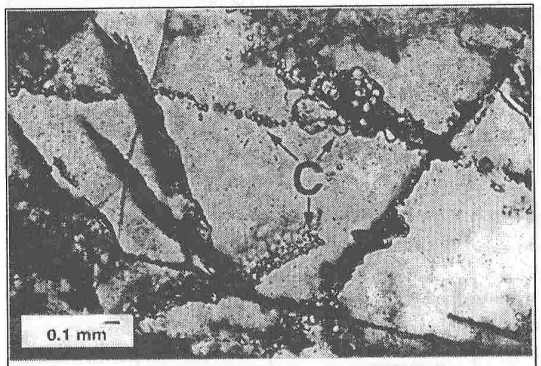

Fig. 3.3.3. Diaplectic quartz glass (clear) from biotite granite inclusion in suevite breccia, Aufhausen, Ries Crater (Germany) appears, with strings of small, high-relief crystals of coesite ("C") (from French, 1998.)

According to Stöffler (1974) and Engelhardt (1990), the stages of shock metamorphism in the impact formations of the Ries impact crater were characterized by plastic deformation and isotropization of minerals, the formation of high-pressure phases and the occurrence of melting phenomena. This classification was based not only on the Ries rocks but also on shock experiments. The pressures and estimated temperatures refer to rocks of approximately granitic mode and composition (Table 1).

References: [1] Engelhardt W. v. (1990): Distribution, petrography and shock metamorphism of the Ejecta of the Ries crater in Germany-a review. *Tectonophysics*, **171**, 259-273; [2] Deutsch, A. (1998) Examples for Terrestrial Impact Structures. In: Mineral Matter in Space, Mantle, Ocean Floor, Biosphere, Environmental Management, and Jewelry (ed. By Marfunin A.S.), *Advanced Mineralogy*, 3, 119-129; [3] Engelhardt W. v., Stöffler D. (1965) Splatflächen im Quarz als Anzeichen für Einschläge grosser Meteoriten. *Naturwissenschaften*, 17, 489-490; [4] Stöffler D. (1972): Deformation and transformation of rock-forming minerals by natural and experimental shock processes: II. Behavior of minerals under shock compression. *Fortschr. Mineral.* **49**, 50-113; [5] Stöffler D. (1966) Zones of the impact metamorphism in the crystalline rocks at the Nördlinger Ries Crater. *Contrib. Mineral. Petrol.*, **12**, 15-24; [6] French B. (1998): *Traces of Catastrophe*, LPI Contribution No. 954, LPI, Houston, 120 p.; [7] Boggs S., Krinsley D.H, Goles G.G., Seyedolali A., Dypvik H., (2001): Identification of shocked quartz by scanning cathodoluminescence imaging, *MAPS*, **36**, 783-793; [8] Stöffler D. (1974): Deformation and transformation of rock-forming minerals by natural and experimental shock processes. *Fortschr. Mineral.*, 49, 256-298; [9] T. Staudacher, K.E. Jessberger, B. Dominik, T. Kristen, A.O. Schaeffer, ^{40}Ar-^{39}Ar of rocks and glasses from the Nördlinger Ries crater and the temperature history of impact breccias, *J. Geophys.* **51**, (1982) 1-11.

3.4. ANALOG STUDIES ON ROCK ASSEMBLAGES DELIVERED TO A PLAIN BY FLOODS, ON EARTH (DUNAVARSÁNY) AND MARS (CHRYSE-PLAINS).

Introduction: Many different kinds of rocks were found by the two Viking space probes and by Pathfinder after their landing on Mars. At first look the objects in the vicinity of the space probes were categorised in two major groups: boulders and moving sediment. The boulders were partly embedded in the desert soil consisting of small particles. The moving sediment was arranged in various shapes, such as dunes, wind flags and ripples. Here we look for analog case on the Earth for transported boulders. Mainly their surface textures were observed on the site. In an analog field work organized in petrology to study rocks transported by Danube to Dunavarsány, Hungary gave similar problem as compared to the situation of Martian Pathfinder's rock observations where on the landing site the floods of the Ares Vallis river transported the rock types of the southern highlands to the Chryse Planitia. However, the locations and relative positions of the rocks in the pile was not comparable to the Martian case. On Eötvös University the 3rd year geologists took part in this field work of petrologic study of pebbles of the polimict gravel in the Dunavarsány mine of U-Pleistocene age.

The locality is south of Budapest. The surface gravel formation of the South Pest Plain Pliocene-Pleistocene Suite has 20-100 m thickness in this region. It consists of the sediments of the terraces of Danube [1]. It contains various rocks from the middle and upper flow of the Danube: quartzite from the Alps, (ca. 500 km of transporting distance), andesite (Miocene age, from the Börzsöny Mts. ca. 50 km transp. dist.), and sedimentary rocks, however, it contains also eclogite, granulite, amphibolite of unknown locality, probably more than 500 or as far as 1000 kilometers of transporting distance.

The samples were collected in the gravel pit of the Aqua Ltd., near Kisvarsány, on a gravel hill. Generally 5-10 cm sized pebbles can be found here, however sometimes some decimeter sized boulders were also found (Fig. 3.4.1.).

Description of the main rock pebble types:
The distribution of the pebble types:

Rock	% in the sample		
quartzite:	36.3%	andesite:	15.7%
limestone:	17.6%	gneiss:	2.9%
marl:	1.9%	amphibolite:	11.9%
granite:	5.9%	sandstone:	7.8%
granulite:	4.9%	conglomerate:	3.9%
		rhyolite:	0.9%

Textures of the main rock types:
Granite: These light tone pebbles are well rounded, only partly weathered rocks. Its texture is subhedral granular. The mineral constituents are feldspar (fresh, euhedral, or subhedral), quartz, micas (they begin to transform to chlorite, or biotite to limonite, some muscovites), garnet (rare small grains) (Fig. 3.4.2.). Among the variants of granites there can be found tourmaline granites with large tourmaline crystals.

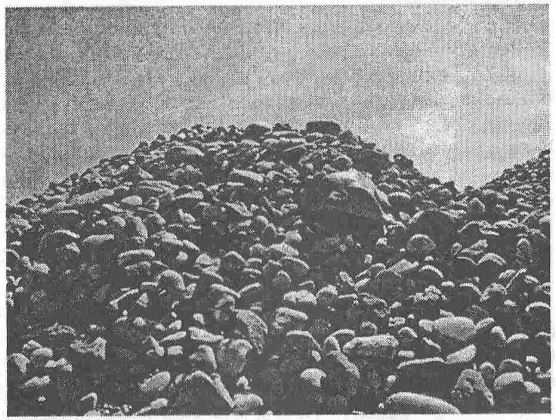

Fig. 3.4.1. The pebble pile in the gravel pit of Dunavarsány.

Rhyolite: There can be found several types of rhyolites in Dunavarsány. Their size, roundness is variable their color is pale violet, but brown and grey also occur. Mineral constituents: feldspar, quartz, biotite and rarely amphibole. One type is the spherolitic rhyolite: it is a light yellow or pale violet rock. There are red spherolites with rounded shape, 1-6 mm sized.

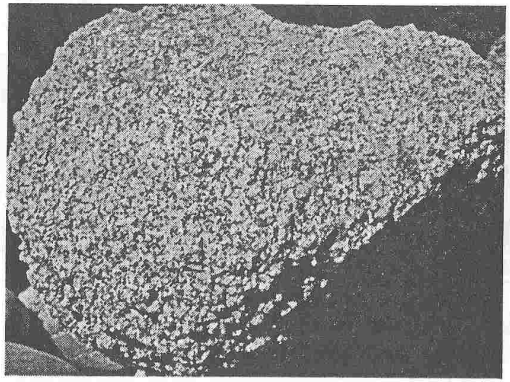

Fig. 3.4.2. Biotite-granite from Dunavarsány. The resolution is similar to that of the best rover cameras and it allows identification of rock type.

Andesite: Brown or grey, rather weathered and rounded rocks. Its main mineral constituents are feldspar and amphibole (Fig. 3.4.3.).

Conglomerate: It is a grey or brown rock containing middle or well assorted quartz grains. Its grains size is 0.5 centimeter in average.

Limestone: Many types can be found in this gravel pit: nummulitic, lithotamniumic, krinoidic, snail or shell rocks. Its size and abrasion is variable and its color is in wide range from white-yellowish to greyish-brown.

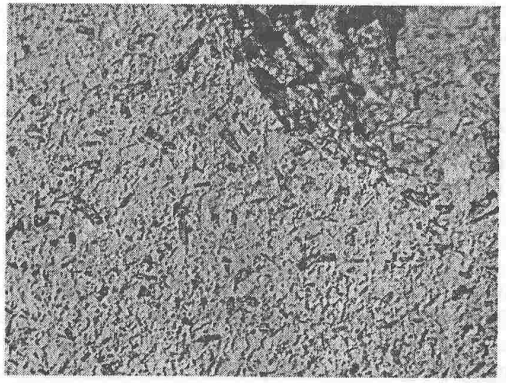

Fig. 3.4.3. Digit-camera resolution allows identification of minerals in the fresh broken fabrics. (Here the larger amphibole laths are visible in the amphibole-andesite texture.)

Gneiss: There are many types of gneisses: garnet, biotite, double-mica containing variants. Their size is changing and they are a little rounded. They are frequently shaly, foliated, banded. Their main constituents are the quartz, feldspar, micas and sometimes sillimanite.

Amphibolite: There are many types in the gravel pit: garnet-amphibolite, banded gneiss-amphibolite. Their shape is isometric or elongated; their textures are directed or folded. Constituents: garnet (spherical claret-colored 1-2 millimeter sized grains); amphibole (it consist of the main mass of the rock); feldspar (white minerals appearing in bands); quartz (small, isometric grains).

Granulite: Light colored, partly rounded specimens with plained or isometric shape, in the 5-30 centimeter size range. Their mineral constituents are quartz, feldspar, garnets (2-3 millimeter sized), kyanite (light blue grains with 1 millimeter size), sillimanites (rarely occurring, elongated, fingerlike minerals with several centimeter length). The grain size is alternating in bands.

Classification of pebbles according to their transporting length in the river: The rock pebbles can be grouped into two groups. These groups are well separated on the basis of the shape and size of the pebbles. In one group there are the well abraded, well rounded smaller (less the 20 centimeter sized) grains. Most of the pebble rock types described occurs in this group.

In the other group we can find the larger pebbles, sometimes boulder sized rocks (they even may reach the 1 meter size). These larger rock fragments are more angular, worse abraded rocks. This group represents only a small part of the transported rocks of the river. Their rock type is mainly andesite (50 %), and much granite, granulite and gneiss boulders occur among them and rarely amphibolite. Sedimentary rock also occurs among them: limestone from Triassic or Jurassic, from Eocene and Miocene, sandstones or sandy limestone.

Considering their rounded and abraded shape the members of the first group could be transported from larger distances. They may origin from older conglomerate which later was re-sedimented and settled here. The members of the second group can not come from farther then some ten kilometers. But only parts of these rock types are known in the near vicinity of the gravel pit or from drilling cores in this region. Probably a mountain was on the surface in the Pleistocene near this place and this mountain has been covered and the basin was filled in by the sediments of various sources since Pleistocene and recently only the boulders represent the remnants of this mountain mixed with the pebbles transported from farther distances by the river.

Planetary comparisons of field works: Rock types on a lunar Apollo expedition or in the MPF landing site are mixed from the near or farther rock fragments delivered on the site by various processes. On the Moon the main process was the impact ejection. On Mars MPF case the flooding of the Ares Valley River was the main transporter of rocks. In any case the distance of transportation could be in the range of some 10s of kilometers till as far as 1000 kilometers. The great variability among the rock types can be seen on the Pathfinder's landing site where various rock surface textures were described [2, 3, 4,]. In the MPF landing site – as on the Dunavarsány gravel pit – both igneous and sedimentary rocks occur. Camera resolution approaches the visual resolution in a field work observer's one. Identification of rock types was increased in the laboratory, in the thin section studies; however the field work estimation is in the range of the space probe camera's resolution capability. The positions on the MPF site are also informative and the stratigraphic relations in a gravel pit may also add some information of the sedimentation process. The field work with preparation from the planetary surface knowledge adds some point of view which will not arise without planetary landers geologic knowledge. These are:

1) Estimation the textures from various distances. (Approaching to the boulder may increase the exactness of the identification of the rock texture.)

2) Identification of minerals in the rock textures. (In terrestrial conditions we may increase the resolution by lupe. Consequence: we must develop small lupe or microscope to the experimental university lander Hunveyor or onto its Husar rover.) However, today the resolution of some digital cameras is comparable to those of lupe.

References: [1] Zsemle F., Török K., Józsa S., Kázmér M. (2001): Granulite pebbles from the Upper Pleistocene terrace of the Danube at Délegyháza, Hungary. *Földtani Közlöny*, **131/3-4**, 461-474.; [2] Basilevsky, A.T.; Markiewicz, W.J.; Thomas, N.; Keller, H.U. (1999): Morphology of the APXS Analyzed Rocks at the Pathfinder Site: Implications for Their Weathering Rate and Distance of Transportation. *LPSC XXX*, #1313, LPI, Houston, (CD-ROM); [3] Bridges, N.T.; Greeley, R.; Kuzmin, R.O.; Laity, J.E. (2000): Comparison of Terrestrial Aeolian Rock Textures to Those at the Mars Pathfinder Landing Site. *LPSC XXXI*, #2066, LPI, Houston, (CD-ROM); [4] Parker, T.J.; Moore, H.J.; Crisp, J.A.; Golombek, M.P. (1998): Petrogenetic Interpretations of Rock Textures at the Pathfinder Landing Site. *LPSC XXIX*, #1829, LPI, Houston.

4.1. TEXTURES OF BASALTS AND BASALTIC CLASTS OF THE NASA LUNAR EDUCATIONAL SET: COMPARISONS TO TERRESTRIAL BASALTS.

Since 1994 we loan and study NASA Lunar Educational Thin Section Set. In this first chapter we tell how these basalts and basaltic clast textures from breccias and soil samples were 1) arranged according to their silicate paragenetic sequences, textural characteristics, and the estimated cooling rates, 2) fitted into a reconstructed tentative TTT-diagram for a lunar basaltic lava flow, 3) compared to those of a terrestrial flow textures (tholeiitic composition).

Introduction: Basaltic textural types, their grain size, crystal morphology are in systematic relation with the cooling rates in the magma body [1]. In an undisturbed magma body from the edges toward the deeper layers gradually slower cooling rates result in gradually coarser textural types. From crystal morphology, paragenetic sequences [2] we can arrange NASA lunar set textures of a 8-10 meters thick lunar basaltic flow [1-5]. according to cooling rates and textural types [6].

We focused on basaltic samples of the lunar set, because Carpathian Basin petrology is rich in different basalts and gabbros for comparisons. From Carpathian Basin basalts we selected an ophiolitic textural series of the Darnó Hill, Heves C., Hungary [7]. Forming a continuous sequence of textures we used parallel both terrestrial and lunar samples [3]. (The following thin sections were used from NASA set: 74220, orange soil; 68501, clasts in soil s.; 14305, clasts in breccia; 72275, clasts in breccia; 12002 porphyritic s.; 70017, poikilitic s.; 12005 poikilitic s.) The reconstructed tentative TTT diagram represents a lunar "average" flow, which solidifies between 1250 and 950 C, contains the textural fabrics of the Fig. 1. sequence, with the cooling rates from glassy quenching 1000 C/min. rate till 0.5-0.05 C/hr. Our tentative TTT-diagram form a common background for detailed basaltic textural studies for students.

Textural sequence of basaltic samples and clasts in NASA lunar educational set: On the basis of the sequence of terrestrial textures we estimated (interpolated) the place (probable original depth) of the lunar set textures in a lunar basaltic lava flow. We also used literature data for cooling rates. The samples in a sequence starting from the greatest cooling rate are:

74220 The "highest" position (the greatest cooling rate) had the orange soil spherules in the **74220**, because their ejection as a lava fountain ([6],[9],[11]) had glass quenching cca. 1000 C/min. cooling rate [12].

68501 Variolitic clast. (We remember from earlier loans, that in NASA Lunar set No. 6. 72275,509 breccia contained a larger vitrophyric-variolitic clast. 72275 is the thin section with the largest surface in the lunar set). Recent (No. 4.) set contains a clast with spherulitic-variolitic texture among the soil grains of **68501.** This clast had second highest cooling rate in our sequence (tentatively: some hundred degrees Celsius per day).

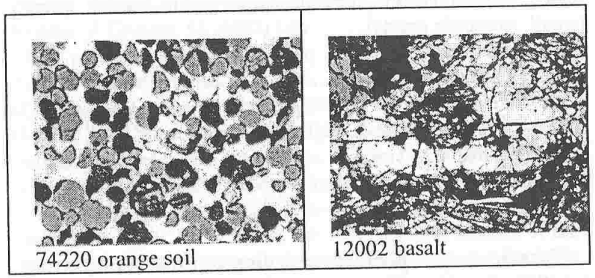

Fig. 4.1.1. Apollo 17 orange soil and Apollo 12 basalt texture. (NASA Lunar Sample set thin section photograph.)

12002 This Apollo 12 porphyritic sample **12002** represents slower initial cooling rate for the large olivine grains and higher cooling rate (wide range) for the surrounding (variolitic) laths of clinopyroxenes and plagioclase feldspars[12]). In a revised model cooling rates may vary from some degrees Celsius to 2000 C/hour [17].

14305 The breccia **14305** contains intergranular type clasts, such representing the third texture in the cooling rate sequence (tentatively: hundred degrees Celsius per week)

72275 The subophitic clast of **72275,**128 breccia represents an even slower cooling. Over breccias all three basaltic samples represent well crystallized beautiful specimens.

70017 This poikilitic sample of **70017** has paragenetic sequence similar to A-11 High Ti- basalts [2] [15], rich occurrence of sector zoned clinopyroxenes. The rich population of ilmenites make dark the thin section: this ilmenite rich specimen has a counterpart near to Darnó Hill (at Szarvaskő), in a gabbro with high ilmenite cont. bw. 8-10 % wt.)

12005 The Apollo 12 poikilitic **12005** sample had the slowest cooling, so this specimen closes our cooling rate series. It contains large, zoned pyroxene oikocrystals with embedded idiomorphic (euhedral) olivine grains of chadacrysts [12].

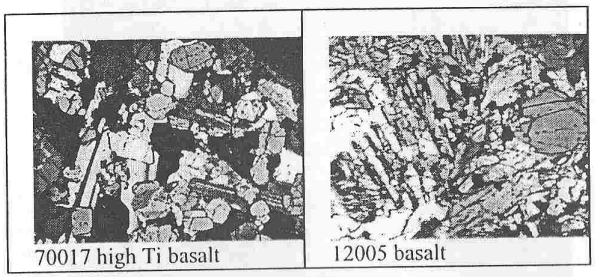

Fig. 4.1.2. Apollo 17 high Ti basalt and Apollo 12 basalt texture. (NASA Lunar Sample set thin section photograph.)

Terrestrial counterpart textures: an ophiolitic sequence of Darno Hill: In the Darnó Hill (basalts and microgabbros) textural sequence of an ophiolite can be found. From the outer edge high cooling rate textures to the bottom of the lava layer (or to the center of a pillow lava "sphere") the following textures represent this series: spherulitic, variolitic, intersertal, intergranular, subophitic, ophitic, poikilitic. [7]. Although important details are different in a terrestrial flow and in a lunar flow (chemical compositions, - e.g. 74220 and 12002 are picritic basalts [5], [10], [16]. - water content can change paragenetic sequence of crystallization for plagioclase feldspar and pyroxene), the main textural characteristics determined by cooling rates remains important basis for comparisons and TTT diagrams.

Cooling rates for lunar and terrestrial basalts and tentative TTT diagram for the lunar basalts: On the basis of experimental determination of the cooling rates and also from TEM measurements of clinopyroxenes both cooling rate sequences and TTT-diagrams were studied and determined [1], [3], [13-15]. The lunar basalt layer was 8-10 meter thick [13] [15]. This thickness is larger, but comparable to pillow lava units as terrestrial pairs. A pillow lava cools during 2 days, but 8-10 meters thick lunar layers cooled for months or years in their inner regions.

In a pillow lava textural sequence only the intergranular texture could be reached because of the quick cooling and smaller lava body size. In the lunar basalt case all textural types in our sequence could be reached. The corresponding cooling rates were given by [3] as 3 C/min. for a vitrophyric, 30 C/hr for a coarser vitrophyric and 3 C/day for a porphyritic Apollo 15 sample.

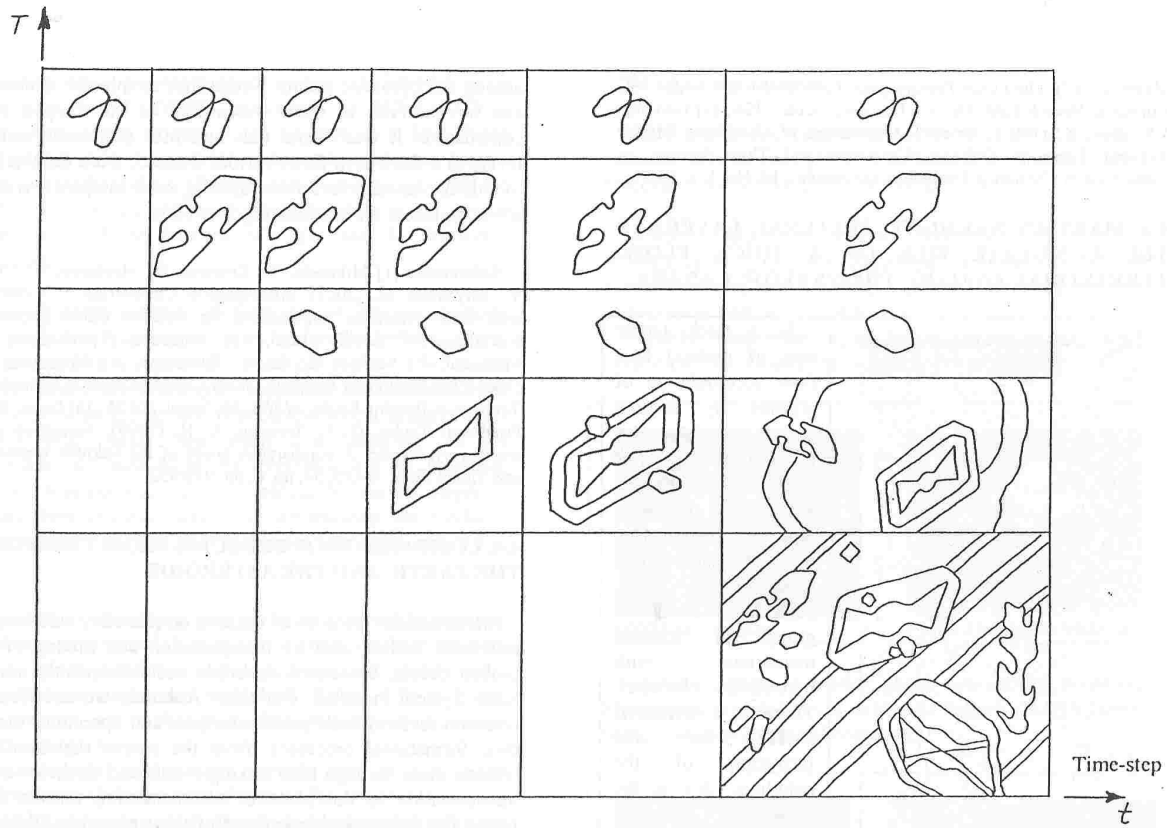

Fig. 4.1.3. Paragenetic sequence of the 70017 NASA Lunar educational set basalt sample. Armalcolite starts the sequence, which is followed by ilmenite, olivine, pyroxene and feldspar.

Data of a pillow lava are in table 4.1.1. as follows: [7]

textural type	cooling rate	depth in a pillow lava	length of cooling time
glassy	45000 - 1800 C / min.	1 centimeter	1 min.
spherolitic	22000 - 1000 C / min.	some centimeters	some minutes
variolitic	1000 - 200 C / min.	decimeter	10 minutes - 0,5 hour
intersertal	200 - 30 C / min.	some decimeters	0,5 - 2 hours
intergranular	0,5C / min.	central region of pill.l.	1 - 2 days

Summary: From lunar basaltic textural characteristics a paragenetic and cooling rate sequence, a tentative TTT-diagram of basaltic lava flow layers were constructed. These data were compared to a terrestrial basaltic flow textural layers.

References: [1] Lofgren, G.E., Donaldson, C.H., Williams, R.J., Mullins, O. (1974): *5th LSC*, 458-460.; [2] Bence, A.E., Papike, J.J. (1972): *3th LSC*, 59-61.; [3] Grove, T.L. (1977): *8th LSC*, 380-382.; [4] Grove, T.L., Bence, A.E. (1977): *8th LSC*, 383-385.; [5] Grove, T.L. et al. (1973): *4th LSC*, 323-325.; [6] C. Meyer: (1987): *The Lunar Petrographic Thin Section Set.* NASA JSC Curatorial Branch Publ. No. 76. Houston, Texas, USA. [7] Józsa S. (2000). Thesis. Eötvös University, Dept. Petrology/Geochemistry, ELTE, Budapest; [8] Szakmány Gy. (1995): The main textural types of igneous rocks. (In Hungarian). Eötvös Univ. Lect. N. Ser. Dept. Petrology.; [9] Delano, J.W., & Livi, K. (1981): Lunar Volcanic Glasses. *GCA* 45, 2137.; [10] Grove, T.L., et al. (1973): *4th LSC*, 323-325.; [11] D.S.McKay, D. S. & Wentworth, S. J. (1992): *Geology of Apollo 17 Landing site, WS.*, LPI Techn. Rep. No. 92-09, Part 1. p.31.; [12] Dungan, M. A., Brown, R. W. (1977): The Petrology of the Apollo 12 Basalt Suite. *Proc. Lunar Sci. Conf. 8th.* 1339.; [13] Grove T. L. (1982): *Am. Min. 67*, 251-268.; [14] McConell, J.D.C. (1975): An. Rev. Earth. Planet Sci. 3. 129.; [15] Nord, G.L., Heuer, A.H., Lally, J.S., Christie, J.M. (1975): *6th LSC*, 601-603.; [16] Walker, D., et al (1974): *5thLSC*, 814-816.; [17] Walker, D., Kirkpatrick, R.J., Longhi, J., Hays, J.F. (1975): *6th LSC*, 841-843.

4.2. COOLING RATE SEQUENCE OF CHONDRULE TEXTURES

Introduction: In order to extend comparisons among planetary materials the cooling rate sequence of the chondrule types were also involved into this study. The cooling sequence of chondrule types as individual melt droplets were reconstructed from the NIPR Meteorite samples from set No. 4.: Yamato-790448,64-5 (LL3 chondrite), Yamato-691,53B-1 (EH3 chondrite) and the Hungarian meteorites (thin sections from the Eötvös University Collection samples): Mezömadaras (L3 chondrite), Knyahinya (L5/6 chondrite) were used to overview the cooling rate sequence of chondrules.

Chondrule textural types: In the chondrites studied all (generally 6 named) types of the glassy (or criptocrystalline), (excentro-)radial, barred, porphyritic (olivine-PO, pyroxene-PP, olivine-pyroxene-POP), granular and poikilitic (pyroxene) chondrule textural types occurred.

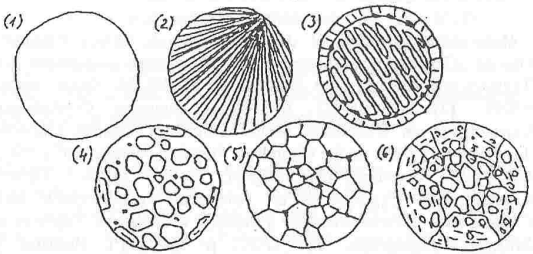

Fig. 4.2.1. The six main chondrule textural types.

Many experimental reconstructions successfully reproduced these textural types in the function of composition, cooling rate, presence or nucleation of olivines and pyroxenes, petrological setting (i.e. partial melts), grain size of the

precursor materials and even such factors as rotating chondrules [1, 2, 3, 4].

One of the most important factors is shape and other is the size [5]. Shape is important, because the spherical body has small place for exhibiting strong gradients in the textures. Sphere is a strong boundary condition. Size is determining the cooling rate very effectively.

The glassy chondrules are frequently occurring among the smaller ones. The smaller the droplet is, the worse is the surface /volume ratio. On the basis of the orange soil cooling rate estimations the glassy spherules could have 1000 C/min cooling rate [7, 8].

The porphyritic chondrules with much glassy mesostasis can be the next in the sequence. Their estimated cooling rates were between 100 C/hour and 2000 C/hour. [4, 6] Last experiments show that they were formed by partial melts of an olivine rich source [1], their cooling rate was in the order of 100 C/hour. However, some excentro-radial types may run parallel with them in this cooling rate sequence. (Not only overcooling results in abrupt crystallization of pyroxene bunch or fascicule but the absence of crystal nuclei.)

Barred chondrules are also in this section in the cooling sequence of chondrule textures [2, 3]. The slower cooling rate types are the poikilitic pyroxene and the granular types. For granular textures between 2 C/hour and 30 C/hour cooling rates were given by [4]. Although unequivocal sequence can not be given, the main lines of cooling sequence could be shown by these 6 types, too. However, we may not miss to mention that we found an extended study from 1981 [9] which concludes that "of 1600 chondrules neither chondrule size nor shape is strongly correlated with textural type".

References: [1] Zieg, M. J.; Lofgren, G. E. (2003): Porphyritic Olivine Chondrules: Constraints on Formation Conditions from Textures and Experimental Simulations. *MAPS*, **38**, Suppl., abstract #5097.; [2] Lofgren, G. E. (1989): Dynamic Crystallization Experiments on Chondrule Melts: Origin of Droplet Chondrule Textures and Limits on the Chondrule Forming Process. *20th LPSC*, p. 698, LPI, Houston; [3] Lofgren, G. E. (1989): Dynamic Crystallization Experiments on Pyroxene-rich Chondrule Melts: Comparison of Experimentally Produced and Natural Textures and Mineral Compositions. *20th LPSC*, p. 582, LPI, Houston; [4] Weinbruch, S.; Buttner, H.; Rosenhauer, M.; Hewins, R. H. (1996): Experimental Constraints on the Lower Limit of Chondrule Cooling Rates. *27th LPSC*, p. 1405. LPI, Houston; [5] Goswami, J. N. (1984): Size dependence of chondrule textural types. 47th Ann. Meteoritical Soc. Meeting. LPI Contribution 537.; [6] Weinbruch, S.; Muller, W. F.; Buttner, H.; Holzheid, A.; Hewins, R. H. (1997): Cooling Rates of Porphyritic Olivine and Excentroradial Pyroxene Chondrules. *MAPS*, **32**, p. A138; [7] Dungan, M. A., Brown, R. W. (1977): The Petrology of the Apollo 12 Basalt Suite. *Proc. Lunar Sci. Conf. 8th.* 1339.; [8] C. Meyer: (1987): *The Lunar Petrographic Thin Section Set.* NASA JSC Curatorial Branch Publ. No. 76. Houston, Texas, USA; [9] Gooding, J.A., Keil, K. (1981): Relative Abundances of Chondrule Primary Textural Types in Ordinary Chondrites and Their Bearing on Conditions of Chondrule Formation. *Meteoritics*, **16**. No. 1. p. 17.;

4.3. MARTIAN NAKHLITE TEXTURAL LAYERS IN THE CUMULATE PILE OF A THICK FLOW: TERRESTRIAL ANALOG: THEO'S FLOW, CANADA.

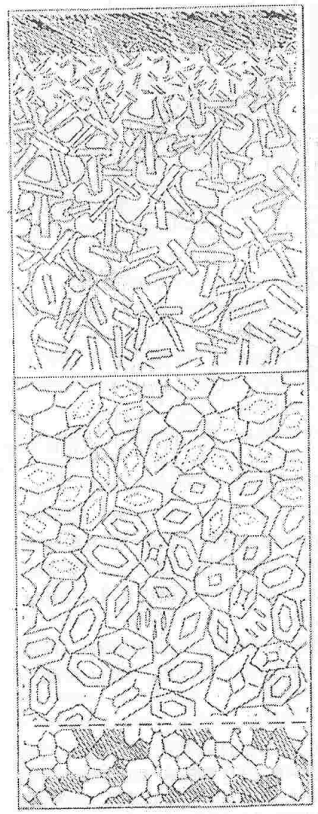

In a thick (some tens of meters) lava flow accumulation of crystals by settling forms cumulate piles in the lower section of the lava column. Martian nakhlites represent this section of the lava flow column [1-3]. Nakhlites form a group of martian meteorites with pyroxenitic character. There is a terrestrial analog for the formation of the nakhlites: this is the ultramafic lava-flow of the Theo's Flow in Canada. The martian meteorite nakhlites have similar petrographic texture to that of the Theo's Flow piroxenites: it consists of piroxene (mainly augite) grains set in a matrix composed of plagioclase needles.

In the melt first pyroxenes were well nucleated. Then the growing pyroxenes formed clusters and settled on the top of the cumulate pile at the bottom of the lava layer. Finally the trapped melt crystallized in the form o the plagioclase needles. These plagioclase needles form bunches between the clinopyroxene crystals. Smaller number of olivines occur among the pyroxene grains. Sometimes simplectite exclusion can be observed in them. According ot the trapped melt composition it was found that nakhlites populated various levels in a thick lava flow, various distance from the top [1]. In a thick planetary lava-flow layering these samples represent lower region of the crystallizing lava body.

References: [1] Mikouchi, T.; Koizumi, E.; Monkawa, A.; Ueda, Y.; Miyamoto, M. (2003): Mineralogical Comparison of Y-000593 with Other Nakhlites: Implications for Relative Burial Depths of Nakhlites. *34th LPSC.* #1883, LPI, Houston; [2] Koizumi, E.; Mikouchi, T.; McKay, G.; Le, L.; Monkawa, A.; Miyamoto, M. (2003): Implication for the Slow Linear Cooling Origin of Vitrophyric Textures in Basaltic Rocks. *MAPS*, **38**, Suppl. #5175.; [3] Lentz, R. C. Friedman; Taylor, G. J.; Treiman, A. H. (1999): Formation of a martian pyroxenite: A comparative study of the nakhlite meteorites and Theo's Flow. *MAPS*, **34**, no. 6, pp. 919-932.

4.4. COMPARISON OF BRECCIAS FROM THE MOON, THE EARTH, AND THE ASTEROIDS.

Introduction: Because of impacts on planetary surfaces, on asteroidal bodies, also by transportation and mixing of the broken debris, bracciated materials occur frequently among Solar System materials. For these materials we can identify common textural description principles and operations during their formational processes: from the source region of the textural units, through their mixing events and on their way of transportation to the place of sedimentation, till the final fusing the formational operations of these materials has many similar characteristics. Terefore they can be described with a common technological type sequence (manufacturing) generally known in ceramics industry.

Breccias from the NASA Lunar Set, NIPR Antarctic meteorite set, chondritic meteorites from Hungary, terrestrial rock samples were compared, their processing steps were concluded in our comparative planetary petrography analog study. Various types of brecciation: early solar nebula mixing and accretion (chondrites), surface impacts (chondrite parent body, lunar, basaltic achondritic), pyroclastic ejection (terrestrial), and repeated reworking (lunar, ancient ceramics) were studied, and the sequence of the main steps of operations (breaking, crushing, transporting, mixing, recycling and final welding or heating) were compared.

Samples: In our studies we used the following samples: **NASA Lunar Set**: 14305, 15299, 65015, 72275, 60025; **NIPR Antarctic Set**: Y-86032 (Lunar regolith breccia), ALH-78113 (aubrite br.), ALH-77256 (diogenite br.), Y-7308

(howardite br.), Y-74450 (eucrite br.), Y-790448 (LL3 chondrite), Y-691 (EH3 chondrite), Y-86751 (CV3); **Chondrites**: Mezömadaras (L3), Knyahinya (L5/6), Kaba (CV3), Mócs (L5); **Terrestrial rocks**: volcanoclastics: basalt-lapilli, Szentbékkálla (Pannonian-/Pleisztocene), pebble conglomerate of Carboniferous is embedded in the pebble congolmerate of the Mecsek Mts. (L. and M. Miocene) embedded.

Main breccia-textures Definitions of breccia textures distinguish two main types: para and ortho-breccias. Para-breccias are matrix-supported: the larger grains "flow" in the matrix. Ortho-breccias are grain-supported and matrix fills the regions between the grains. Breccia-in-breccia textures refer textures with fractal type grain size hierarchy. In the descripitons we used these characteristics and the breaking, crushing, transporting, mixing, welding or heating stages in the formation process. Grain size distributions, the modality and the sorted nature of the clasts were also measured in this study.

Chondrites: Chondrites were probably accreted in a cosmic sedimentation process [1], they can be considered accretionary breccias. More chondrites are para-breccias (with more matrix, chondrules are surrounded with them, Kaba, Y-86751) than ortho-breccias, where chondrules frequently touch each other (Mezömadaras, Knyahinya).

Two asteroidal evolutionary periods may produce other characteristics of the brecciated texture for chondrites. During 1) chondrite accretion stage chondrule-breaking by collisions are proved by the occurrence of broken chondrules (Y-790448, Mezömadaras) [2,3]. Other broken chondrite constituents are also known in chondrites.

The 2) period is the stage when rocks were exhibited on the surface of the parent body, and impacts could break, mix and weld together chondritic pieces with different metamorphic type. Brecciated chondrite Knyahinya shows textural evidences of such breaking and mixing. It is also known that breccia-in-breccia texture occurs in chondrites (Cangas de Onis, [4]).

Achondritres: Basaltic achondritic rocks of the differentiated asteroidal bodies are exposured on the surface: the suffered impacts formed monomict or polymict breccias. The NIPR set achondrite breccias (ALH-77256 (diogenite br.), Y-7308 (howardite br.), Y-74450 (eucrite br.), have less crushed/mixed para-breccia texture than most lunar breccias probably because smaller number of impact episodes.

NASA Lunar samples:

60025 anorthosite sample formed by mechanical mixing of cumulate anorthosites [5,6]. Anorthosites are the only ortho-breccias in the NASA Lunar Set. (Fig. 1A.)

14305 Fra Mauro Breccia with breccia-in-breccia texture shows a cycle in the "manufacturing" sequence: the repeated events breaking and welding together. Many regions have para-breccia texture. (Fig. 4.4.1B.)

15299 Regolith breccia (para-breccia) is similar to Y-86032 lunar meteorite. Glassy matrix marks hot welding.

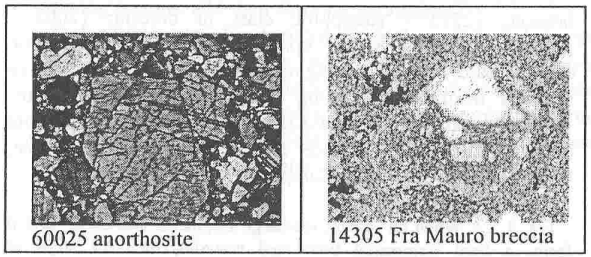

Fig. 4.4.1. Apollo 16 crushed anorthosite and Apollo 14 Fra Mauro breccia with breccia-in-breccia texture. (NASA Lunar Sample set thin section photograph.)

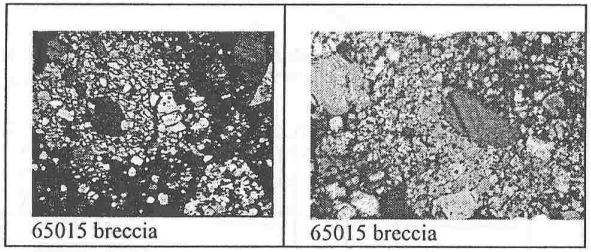

Fig. 4.4.2. Apollo 16 polymict breccia: impact melt glass recrystallized in metamorphism (poikilitic region) [7]. (NASA Lunar Sample set thin section photograph.)

65015 Impact melt breccia, although poikilitic in many regions, but it has a para-breccia texture (Fig. 4.4.2.)

72275 consists of many rock-fragments from the lunar highlands. This para-breccia has two parts: lighter one has lower, darker side has higher matrix/fragment ratio (Fig. 4.4.3.)

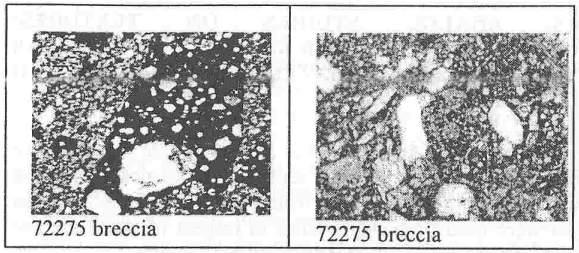

Fig. 4.4.3. Apollo 17 para-breccia which shows breccia-in-breccia regions. (NASA Lunar Sample set thin section photograph).

Terrestrial fragmentary rocks: Pyroclastic rocks were sedimented in a hot state and welded together. Broken fragments wer formed during their transport to the eruption place. One stage event formed their frequently para-breccia like texture, but ortho-brecciated textures also occur (Szentbékkálla, Balaton Highlands, Hungary).

Some sedimentary rock textures exhibit good counterparts for comparisons with the fragmentary aggregated textures we study. In pebble-conglomerates from L. and M. Miocene of Mecsek Mts. Southern Hungary we can find also pebble conglomerates from the Carboniferous. Although the transport mechanism is different from the impact or volcanic type ones, the breccia-in-breccia texture is exhibited in these textures. This is an ortho-breccia. It aggregated in cool state.

Comparisons, conclusions, benefits for technology students: Textural characteristics witness formation processes both for natural and industrial materials. In our study we compared textures and the sequence of the operations were mapped for the samples of Solar System materials The work is fascianting for students and help to recognize the comparable effects between natural and technogical processes.

References: [1] Kracher, A., Keil, K., Kallemeyn, G.W., Wasson, J.T., Clayton, R.N., Huss, G.I. (1985): The Leoville (CV3) Accretionary Breccia. *Journ. Geophys. Res.*, **90**, D123.; [5] Metzler K., Bischoff, A., Stöffler, D. (1992). *Geochim. Cosmochim. Acta,* **56**, 2873; [3] Scott, E.R.D., Rubin, A.E., Taylor, G.J., Keil, K. (1984): *Geochim. Cosmochim. Acta,* **48**, 1741; [4] Williams, C.V., Keil, K., Taylor, G. (2000): Breccia within Breccia in the Cangas de Onis Regolith Breccia: Implications for the History of the H Chondrite Parent Body Regolith. *Chem. Erde*, **60**, 269; [5] C. Meyer (1987): *The Lunar Petrographic Thin Section Set.* NASA JSC, Cur. Br. Publ. No. 76. Houston, [6] Ryder, G. (1982): *Geochim. Cosmochim. Acta,* **46**, 1591; [7] Albee, A.L., Gancarz, A.J., Chodos, A.A. (1973): *4th LSC.* 24.

4.5. ANALOG STUDIES ON TEXTURES: COMPARISON OF LUNAR BASALTS AND BRECCIAS WITH INDUSTRIAL MATERIALS OF STEELS AND CERAMICS.

Introduction: Analog studies play important role in space materials education. Various aspects of analogies are used in our courses. In this year two main rock types of NASA Lunar Set were used in analog studies in respect of processes and textures with selected industrial material samples.

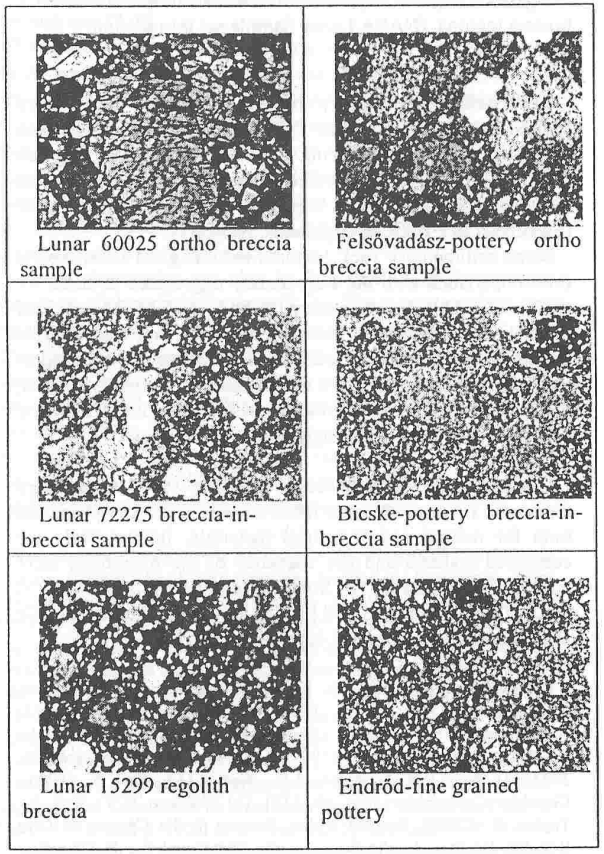

Fig. 4.5.1. The ortho breccia texture (upper row) and the breccia in breccia texture (lower row) in lunar breccia and in a pottery ceramics sample.

For breccias and basalts on the lunar side, ceramics and steels were found as analogs on the industrial side. Their processing steps were identified on the basis of their textures both in lunar and in industrial groups of materials.

Samples: In our studies we used the following samples: NASA Lunar Set: A) **Breccias**: 14305 - breccia-in-breccia texture; 15299 - regolith (para)-breccia, 65015 - impact melt (para)-breccia, poikilitic; 72275 - para-breccia, 60025 - mechanical mixing of cumulate anorthosites, ortho-breccia; B) **Basalts**: 74220 - fast cooling rate, lava fountain droplet [1]; 68501 – clasts in breccia, variolitic, 72275 - spherulitic-variolitic clast in breccia; 14305 - intergranular type clasts in breccia; 72275 - subophitic clast in breccia; 12002 - porphyritic sample; 70017 - ophitic sample; 12005 - poikilitic sample (basalts are in cooling rate sequence). The comparative samples from manufacturing industry. **Ceramics**: Bicske-sample (pottery), Felsővadász-sample (pot.), Szécsény-sample (pot.), and Szarvas-Sample (pot.) **Steels**: perlite-sample, bainite-sample, martensite-sample.

Fig. 4.5.2. When an impact rearrange fragments and clasts, and it forms a final fragmental brecciated material, then the steps of transformations in the impact process (a) are analog in many respects with those of the ceramic industry manufacturing process (b).

Ceramics and breccias: For industrial materials the sequence of the main steps of operations were followed in textural formation (breaking, crushing, transporting, mixing, recycling and final welding or heating).

Impacts always formed brecciated rocks and soils on the Moon. It is interesting to compare the main events during an impact process and in a ceramic manufacturing technology. Impact crush the target rocks, heat up them and during the ejecting process fragmented materials are mixed and collisionally fragmented again. In the ejecta blanket sedimentation process begins the long term cooling and welding together process. Lower layers are under the pressure of the superposed layers. Some parts of the impact and target material melt and special breccias develop.

Basalts and steels - cooling rate: Analog study for lunar basalts made it possible to arrange them in cooling rate sequence. However, for industrial materials the hardening in the steel industrial textures form a sequence of the main steps of operations also according to the cooling rate of the heated steel samples. We can follow both the process and the textures formed in the TTT diagrams.

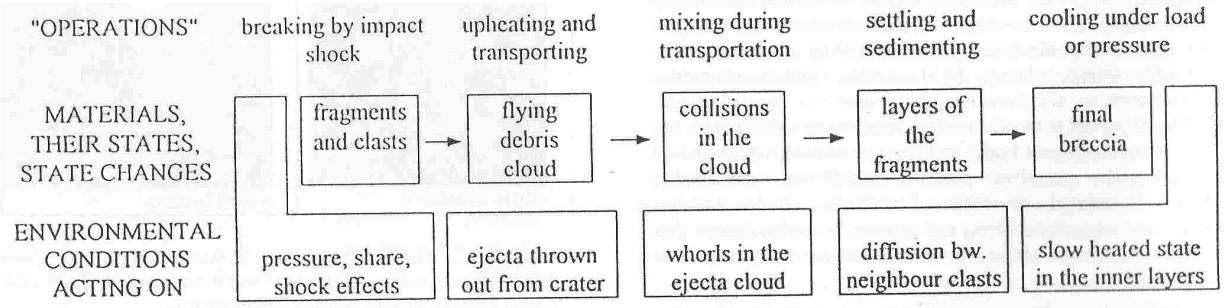

Main operations in the breccia formation: from breaking, transport and mixing through sedimenting till the slow cooling under the pressure of local superposed layers.

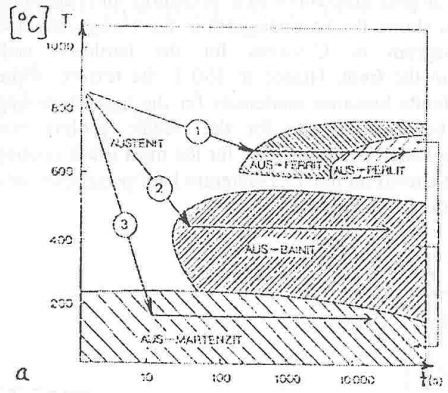

Fig. 4.5.3. Comparison of textural analogs between steels produced by hardening via heating and cooling (in solid state) with various cooling rates and basalt-textures also produced by decreasing cooling rates, (however from a molten state). The "C-rurves" of steels (a).

Discussion: Materials from nature and from manufacturing has common and distinct characteristics. One of their main characteristic is their texture and formation process. The relations between formation process and the produced textural variants are better known for industrial materials. But natural processes are also "mapped" and the relation are summarized in "material maps" like TTT, pT, cT and many other diagrams. If students learn planetary and industry materials parallel, then

1) they have exciting insight to far and exotic topics,

2) they get acquainted with planetary processes and manufacturing processes parallel

3) they get acquainted material maps both with microscope studying textures and their forming parameters,

4) functions may be deduced from the relations between textures and manufacturing steps. This way lunar sample analog studies with industrial counterparts suggest the recognition of steps in formation of other complex material systems and this will initiate their own experiments and studies on more complex materials, too.

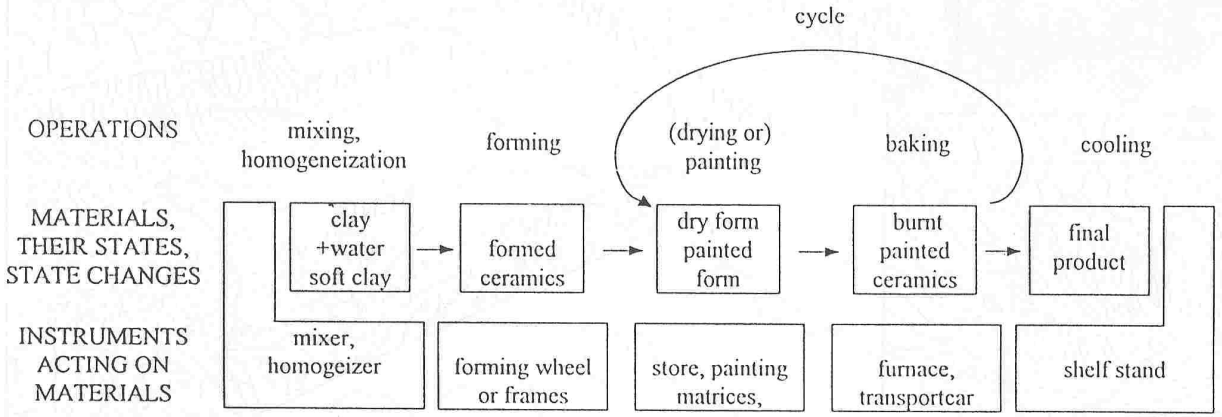

Main operations in the ceramics industry: from clay mixing and homogenization through forming, painting and baking.

This way lunar sample analog studies with industrial counterparts sugest them recognition of steps in formation of other complex material systems and this will initiate their own experiments and studies on more complex materials, too.

Summary: In our analog studies NASA lunar samples were compared with the petrography-manufacturing technology conclusions on their formation processes and textures. This study was not only for planetary science students but for technology students, who has larger background on industrial materials and manufacturing. It was recognized by students that such comparative petrographic study has mutual benefit: possibility to see wider range of formation processes then in the disciplinary studies (only geology and only industry). This work also focuses a valuable type of use of the NASA Lunar Set in planetary materials education.

References: [1] Meyer, C. (1987): *The Lunar Petrographic Thin Section Set.* NASA JSC Curatorial Branch Publ. No. 76. Houston, USA; [2] Bérczi Sz., Földi T., Kubovics I., Lukács B., Varga I. (1997): Comparison of Planetary Evolution Processes Studying Cosmic Thin Section Sets of NASA and NIPR. In *Lunar and Planetary Science XXVIII*, LPI. Houston, p.101. [3] Bérczi Sz., Józsa S., Kabai S., Kubovics I., Puskás Z., Szakmány Gy. (1999): NASA Lunar Sample Set in Forming Complex Concepts in Petrography and Planetary Petrology. In *Lunar and Planetary Science XXX*, #1038, LPI, Houston (CD-ROM); [4] Bérczi Sz., Józsa S., Szakmány Gy. Dimén A., Deák F., Borbéi, F., Florea N., Peter A., Fabriczy A., Földi T., Gál A., Kubovics I., Puskás Z., Unger Z. (2001): Tentative TTT-diagram from Textures of Basalts and Basaltic Clasts of the NASA Educational Set: Comparisons to Terrestrial Basalts. *26th NIPR Symposium Antarctic Meteorites*, Tokyo, 7; [5] Bérczi Sz., Szakmány Gy., Józsa S., Kubovics I., Puskás Z., Unger Z. (2003): How We Used NASA Lunar Set in Planetary and Material Science Studies: Comparison of Breccias from the Moon, Earth, Asteroids and Ancient Ceramics by Textures and Processes. In *Lunar and Planetary Science XXXIV*, #1115, LPI. Houston (CD-ROM); [6] Bérczi Sz. (1985): *Technology of Materials I.* (Lecture Note Series of Eötvös University. in Hungarian), Budapest; [7] Bérczi Sz. (1993): Double Layered Equation of Motion: Platonic and Archimedean Cellular Automata in the Solution of the Indirect Von Neumann Problem on Sphere for Transformations of Regular Tessellations. *Acta Mineralogica et Petrographica, Szeged.* **XXXIX**. p.96-117. [8] Szakmány Gy. (1996): Petrographical investigation in thin section of some potsherds. In: Makkay, J.- Starnini, E.- Tulok, M: *Excavations at Bicske-Galagonyás (part III). The Notenkopf and Sopot-Bicske cultural phases.* - Società per la Preistoria e Protostoria della Regione Friuli-Venezia Giulia, Quaderno 6. Trieste, 143-150; [9] Bérczi Sz., Čech V., Józsa S., Szakmány Gy., Fabriczy A., Földi T., Varga T. (2005): How we used NASA Lunar Set in planetary material science analog studies. In *Lunar and Planetary Science XXXIV*, #1282. LPI, Houston, (CD-ROM);

Fig. 4.5.3. (b) The corresponding basaltic textural field with lines of cooling rates. (c) Main textural regions in the T (temperature)-T (time) transformation diagram with textural regions of various hardened steels.

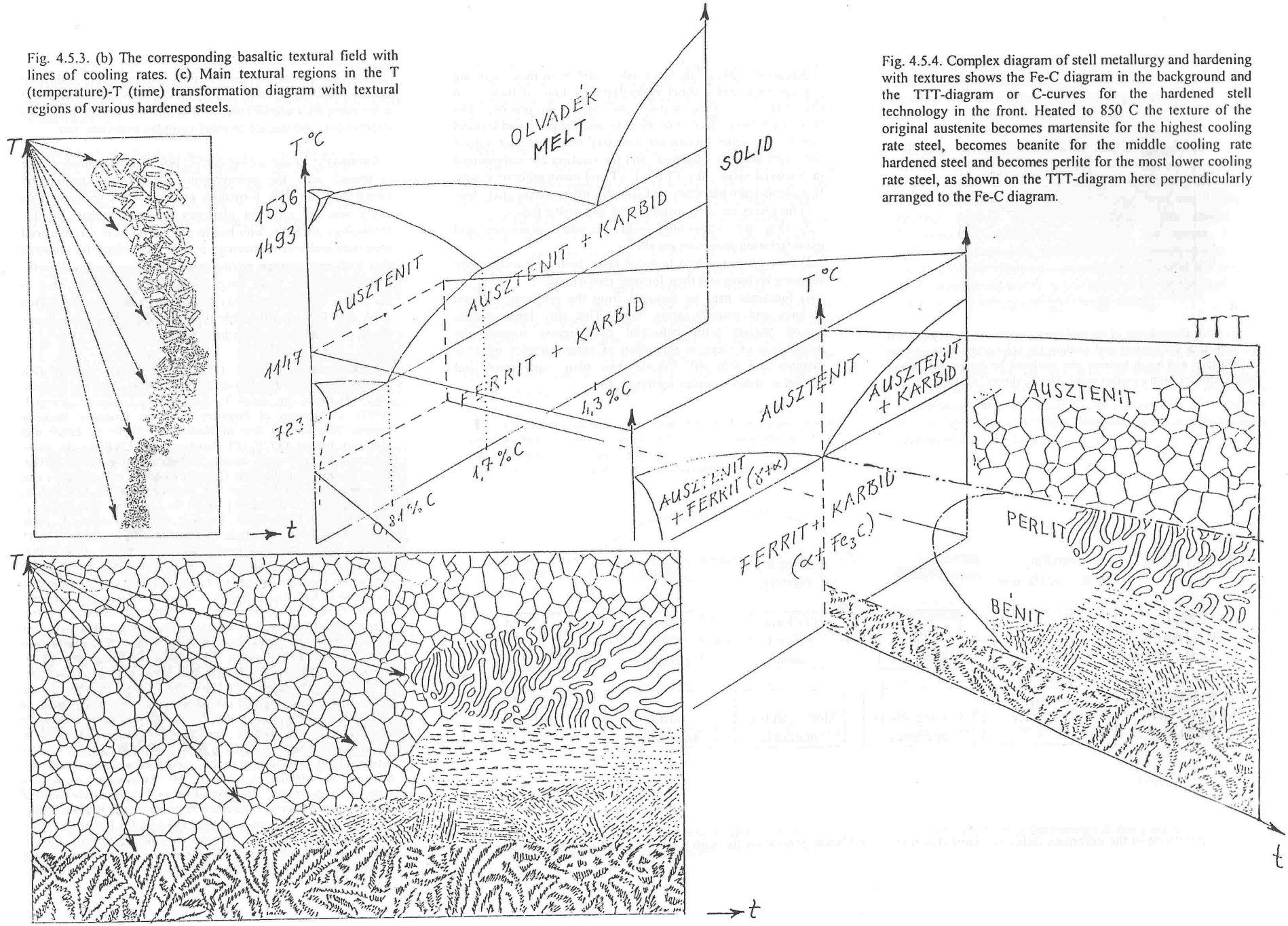

Fig. 4.5.4. Complex diagram of stell metallurgy and hardening with textures shows the Fe-C diagram in the background and the TTT-diagram or C-curves for the hardened stell technology in the front. Heated to 850 C the texture of the original austenite becomes martensite for the highest cooling rate steel, becomes beanite for the middle cooling rate hardened steel and becomes perlite for the most lower cooling rate steel, as shown on the TTT-diagram here perpendicularly arranged to the Fe-C diagram.

MAP OF LOCALITIES WITH PLANETARY ANALOG MATERIALS AND MORPHOLOGIES FROM EUROPE STUDIED IN THIS (9) VOLUME OF CONCISE ATLASES.

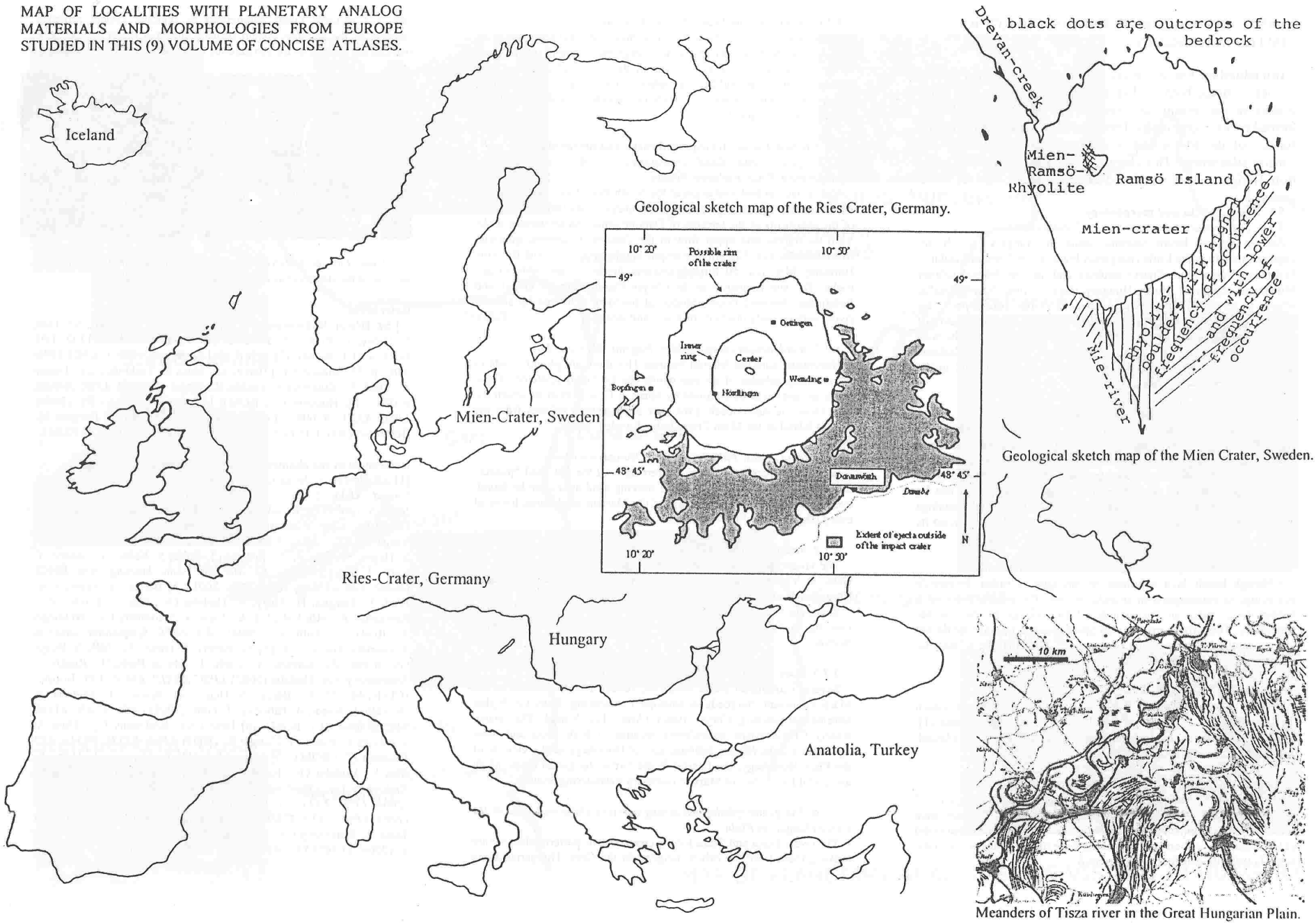

Geological sketch map of the Ries Crater, Germany.

Geological sketch map of the Mien Crater, Sweden.

Meanders of Tisza river in the Great Hungarian Plain.

PLANETARY ANALOG TERRAINS AND ROCKS VISITED IN HUNGARY.

Introduction: For university education the planetary analog studies embrace both studies of various materials, and their studies in the terrain, an overview of the processes which formed rocks, morphology. Previously the lander works on the surface of the Moon and Mars were also involved to our concise atlas works. This chapter shows analog sites and rocks from Hungary which we visited and specimens collected from.

5.1. Igneous rocks and morphology

5.1.1. Shergottite analog rock-series: Szentbékkálla.

Among several basalt volcanic units in Hungary, which are localized mostly in the Little Hungarian Plain, in the Northern-Balaton Mountains region (in Trans-Danubia) and in the Nógrád-Gömör Mountains region in North Hungary there is one, Szentbékkálla, where a series of ultramafic inclusions form counterparts for shergottites. Mantle xenoliths can be found especially in the quarry of the Szentbékkálla village [1]. (Other sources of alkaline basalts with mantle xenoliths and other mafic inclusions in Northern-Balaton Mountains region are Kapolcs, Szigliget, Mindszentkálla and in the Little Hungarian Plain: Sitke.)

5.1.2. Basalt eruption center: Hegyestű, N. Balaton Mts.

Basalt lave erupted at several points of the Tapolca Basin in the North-Balaton Mountains region. Some of them were excavated and mined till the 20th century. Among these rocks the most beautiful outcrop is the Hegyestű Open Air Museum, where the cross section of the eruption center and the streamlines of the erupting lava can be admired with the remnant lava columns. These rocks may be analogs to some hexagonal columnar broken boulders imaged by Spirit on its route in the Gusev crater.

5.1.3. Andesite eruption lava columns: Bér, Cserhát Mts.

Although basalt lava columnar morphology is rather frequently occurring, its counterparts in andesite is rare. The analog site is in a hidden forest place in the vicinity of Bér village in the Cserhát Mountains. These rocks may be also Spirit analogs, because we do not know exactly the composition of the rocks, both may be of basaltic and andesitic one on Mars.

5.1.4. Phonolite from the Mecsek Mountains.

Venera 13 found such high K rock type on Venus. In Hungary such Venusian analog rocks can be found at the Mecsek Mountains [1]. There are quarries at Hosszúhetény and Vasas in the Eastern Mecsek Mts. and at Szászvár in the Northern Mecsek Mts.

5.1.5. High-Ti gabbro from Szarvaskő, Bükk Mountains.

High-Ti basalts were found both on Apollo 11 and on Apollo 17 landing site. Sometimes over the 10 weight percent Ti abundance these rocks has counterpart among Hungarian gabbros from Szarvaskő [2]. Various gabbros and microgabbros were mined at Tardos, and the high-Ti wehrlite was found at Szarvaskő.

5.1.6. Ophiolite from Darno Hill, Bükk Mountains.

In the Darnó Hill (basalts and microgabbros) textural sequence of an ophiolite can be found. From the outer edge high cooling rate textures to the bottom of the lava layer (or to the center of a pillow lava "sphere") the spherulitic, variolitic, intersertal, intergranular, subophitic, ophitic, poikilitic, textures represent analogs to lunar cooling textural layers [3].

5.2. Eroded, fluvial, transported rocks and morphology

5.2.1. River and flood transported boulders and gravels: Dunavarsány, South Budapest Region.

The surface gravel formation at the South Pest Plain, Dunavarsány, with Pliocene-Pleistocene age, with thickness of 20-100 m consisting of the sediments of the terraces of Danube inhabited by various rocks from the middle and upper flow of the Danube. Examples: quartzite from the Alps, (ca. 500 km of transporting distance), andesite from the Börzsöny Mts. (ca. 50 km transporting distance), and sedimentary rocks. The site is analog to the Chryse Plains where Viking-1 and Pathfinder observed flood transported boulders delivered by ancient rivers with recently dry beds of Kasei and Ares [4].

5.2.2. Wind formed sharp pebbles: Nógrád, Börzsöny Mts.

Northwest from the Nógrád Fortress Hill there are plough-fields in which sharp pebbles of ice-age winds can be found scattered. These rocks are analog to those found by Spirit in Gusev crater of which the best known is Adirondack. (We have analog sharp pebbles from the Ramsö Island of the Mien Crater Lake, Sweden, too.)

5.2.3. Sand dunes: Fülöpháza, Great Hungarian Plain.

West from Kecskemét there are remnants of the old sand "puszta" in the Great Hungarian Plain. There moving sand dunes can be found, even today. They are counterparts of the Martian sand dunes found at every landing sites.

5.2.4. Red dunes and rocks: Gánt.

The landscape is rather desert like in an open pit bauxite mine of Gánt, in Vértes Mountains, Hungary. The broken rocks seem as if Hunveyor landed inside a crater.

Sharp outcrops, rolling rocks downward on the slope and the valleys meeting in the central depression all are similar to a fresh crater interior.

5.2.5. River meanders in the Great Hungarian Plain.

Several Carpathian Basin rivers are terrestrial counterparts of the Martian ancient riverbeds downslope meandering from the higher terrains surrounding Chryse Basin (Ares, Tiu, Simud, Shalbatana, Kasei). Characteristic meandering features of both Tisza and other rivers (of Körös, Maros, Szamos, and of Hortobágy in the vicinity of the Plain Hortobágy, the Puszta) in the Great Hungarian Plain [4] all are useful for studies of Martian planetary meandering analogs.

5.2.6. The geomorphological setting of rivers Duna and Tisza in the Great Hungarian Plain.

The rivers Duna and Tisza form a characteristic pattern when we are looking them from the orbital heights. In the Great Hungarian Plain this is a tectonic Lunar counterpart as regional system probably because of the fracture system beneath the lava layers of the lunar mare in the vicinity of the Aristarchus crater and Prinz crater.

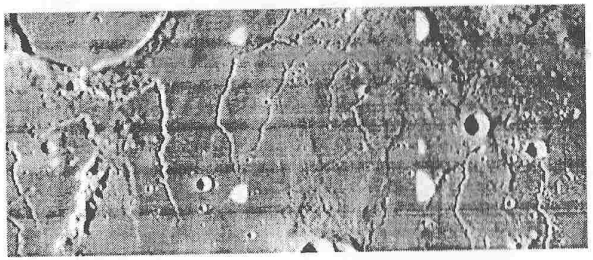

The Lunar Orbiter-4 H151 image about the Rima Prinz system in the vicinity of the Aristarchus crater on the Moon.

References:

[1] Sz. Bérczi, B. Drommer, V. Cech, S. Hegyi, J. Herbert, Sz. Tóth, T. Diósy, F. Roskó, T. Borbola. (1999): *LPSC XXX*, #1332, LPI, Houston (CD-ROM); [2] Bérczi Sz., Lukács B. (1996): KFKI-1996-08/C. p. 23. Budapest; [3] Bérczi Sz., Józsa S., Szakmány Gy., Dimén A., Deák F., Kubovics I., Puskás Z., Unger Z.(2002): *LPSC XXXIII*, #1024, LPI, Houston (CD-ROM); [4] Józsa S., Bérczi Sz. (2004): *LPSC XXXV*, #1608, LPI, Houston [5] Rakonczai J., Hargitai H., Bérczi Sz. (2001): In *LPSC XXXII*, #1507, LPI, Houston (CD-ROM).

References of the chapters in this concise atlas (9) booklet:

[1] Sz. Bérczi, S. Józsa (2003) *Acta Mineralogica et Petrographica, Szeged*, **XLIV**. 57-61; [2] Bérczi Sz., Török K., Gál- Solymos K., Józsa S. (2001) *LPSC XXXII*, #1078, LPI, Houston (CD-ROM); [3] Bérczi Sz., Cech V., Józsa S., Szakmány Gy., Fabriczy A., Földi T., Varga T. (2005) *LPSC XXXVI*, #1282. LPI, Houston (CD-ROM); [4] S. Hegyi, Sz. Bérczi, Zs. Kovács, T. Földi, S. Kabai, V. Sándor, V. Cech, F. Roskó (2001): *64. Met. Soc. Ann. Meeting*, Abst #5402, (*Rome, Vatican City*, 10-15. Sept, 2001) [5] Bérczi Sz., Fabriczy A., Földi T., Hargitai H., Hegyi S., Hudoba Gy., Illés E., Kovács Zs. , Kereszturi A., Mörtl M., Sik A., Józsa S., Szakmány Gy., Weidinger T., Roskó F., Tóth Sz. (2004) *28th NIPR Symposium Antarctic Meteorites*, Tokyo, p. 6. [6] Sz. Bérczi, T. Diósy, Sz. Tóth, S. Hegyi, Gy. Imrek, Zs. Kovács, V. Cech, E. Müller-Bodó, F. Roskó, L. Szentpétery, Gy. Hudoba (2002) *LPSC XXXIII*, #1496, LPI, Houston (CD-ROM); [7] Sz. Bérczi, S. Hegyi, Zs. Kovács, E. Hudoba, A. Horváth, S. Kabai, A. Fabriczy, T. Földi (2003) *LPSC XXXIV*, #1166, LPI, Houston (CD-ROM); [8] Bérczi Sz., Szakmány Gy., Józsa S., Kubovics I., Puskás Z., Unger Z. (2003) *LPSC XXXIV*, #1115, LPI, Houston (CD-ROM); [9] Mörtl M., Földi T., Hargitai H., Hegyi S., Illés E., Hudoba Gy., Kovács Zs., Kereszturi A., Sik A., Józsa S., Szakmány Gy., Weidinger T., Toth Sz., Fabriczy A., Bérczi Sz. (2004) *LPSC XXXV*, #1214, LPI, Houston; [10] Józsa S., Bérczi Sz. (2004) *LPSC XXXV*, #1608, LPI, Houston (CD-ROM); [10] Bérczi Sz. Józsa S., Szakmány Gy., Kubovics I., Puskás Z., Fabriczy A., Unger Z. (2004) *LPSC XXXV*, #1246, LPI, Houston (CD-ROM).

Szentbékkálla

Bér

Nógrád: Hunveyor-4

Nógrád-Gömör Mts.

Darnó Hill

Szarvaskő

Nógrád

Bér

Duna

Tisza

Pécsbánya: Hunveyor-8

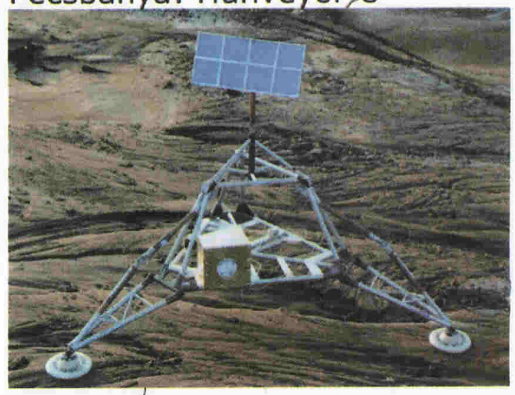

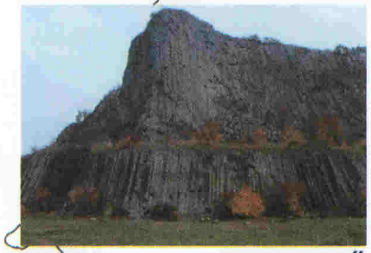

Hegyestű

Hortobágy

Gánt

Dunavarsány

Szentbékkálla

Hegyestű

Balaton

Gánt

Fülöpháza

Great Hungarian Plain

Fülöpháza

Mecsek Mts.

Hosszúhetény

Pécsbánya

Szentbékkálla: Husar-2

MAP OF PLANETARY ANALOG SITES VISITED IN HUNGARY

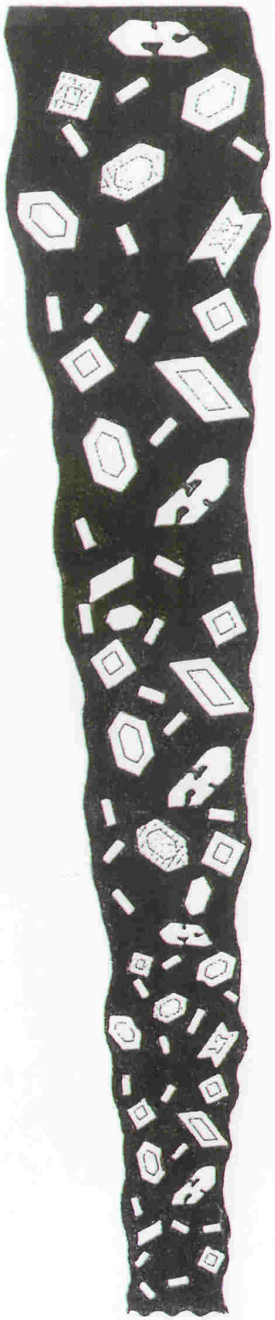

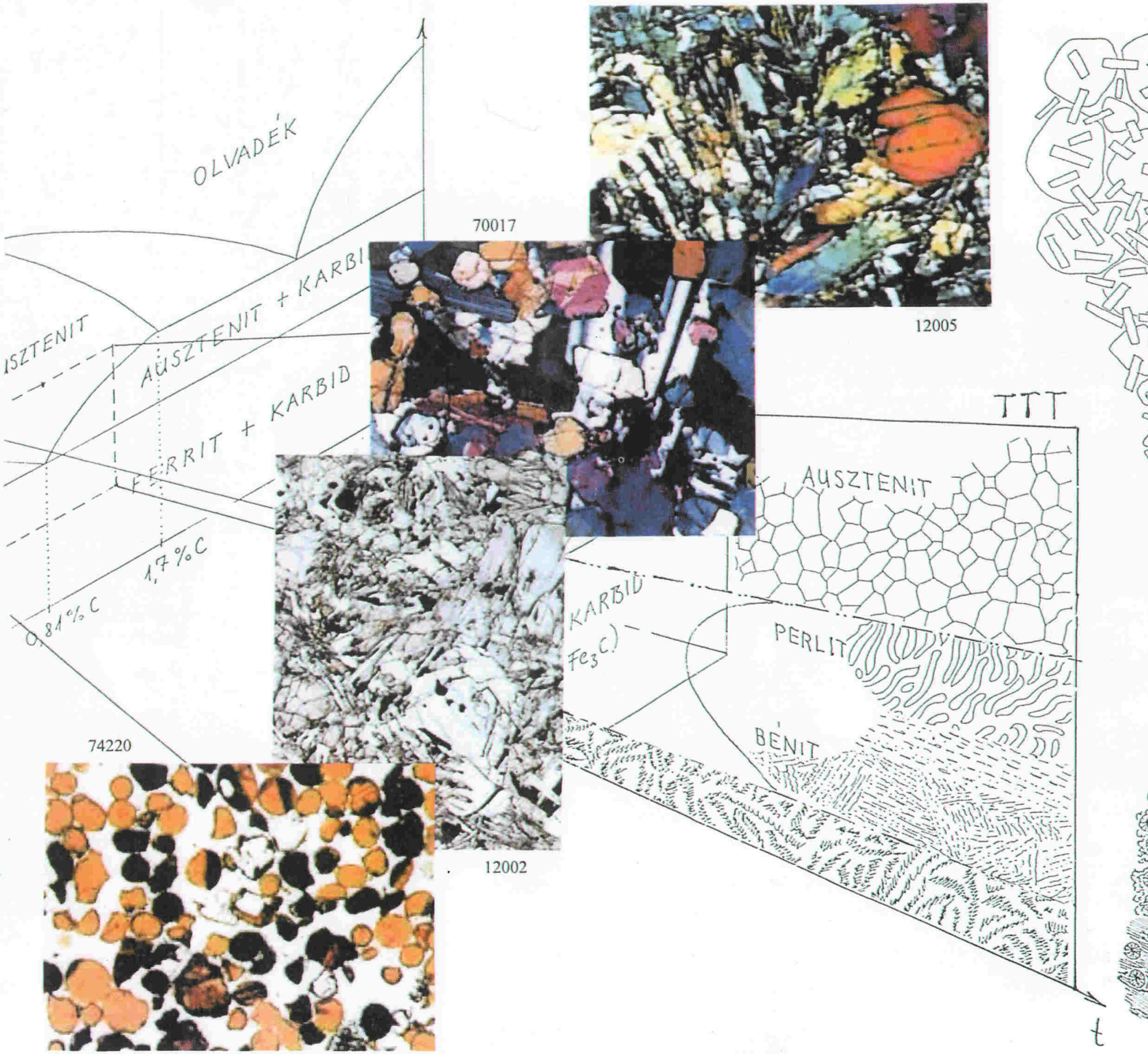
OLVADÉK
AUSZTENIT + KARBI
ISZTENIT
FERRIT + KARBID
0,81 % C
1,7 % C
70017
12005
TTT
AUSZTENIT
KARBID
Fe3C)
PERLIT
BÉNIT
74220
12002
t